# Bolted circular flange connections under static bending moment and axial force

M. Couchaux, Mohammed Hjiaj, I. Ryan, A. Bureau

# Bolted circular flange connections under static bending moment and axial force

**PAR M. COUCHAUX, M. HJIAJ, I. RYAN, A. BUREAU**

***Abstract***

The available design rules to evaluate the force distributions in the tension and the compression parts of bolted circular flange connections under bending moment and axial are often based on the beam theory which is not adequate. The aim of this paper is to propose an analytical model for the calculation of the static resistance of bolted circular flange connections subjected to a combined bending moment and an axial force considering the influence of the joint ductility. An analytical model is also proposed to evaluate the stiffness of the tensile and the compressive parts of the connection and thus its initial rotational stiffness. The results obtained via the proposed analytical model are compared favourably against experimental tests and numerical simulations.

## 1. *Introduction*

Bolted circular flange connections are used in tubular members such as chimneys, pylons for wind turbines and ski-lift installations. Most of these connections should be designed for a combination of bending moment and axial load. Several models have been proposed to evaluate the tensile resistance of bolted circular flange connections under tension ([1], [2], [3], [4]). The L-stub model has also been developed to predict the resistance of the tensile part in connections subjected to combined loading ([5], [6], [7]).

Two types of model have been developed to evaluate the static resistance of bolted circular flange connections subjected to a bending moment and/or an axial force. In the first group of models, which are based on elastic analysis ([6], [8], [9]), the ultimate limit state is assumed to be attained when the resistance of the most critical component of the connection (tensile or compressive) is reached. This approach does not always reflect the observed ultimate behaviour of the connection as other components may possibly reach their full ultimate state before

complete failure of the joint. However, for non-ductile joint (tube-wall buckling, premature bolt failure in tension), this assumption is not far from the experimental and numerical observations [10].

Stamatopoulos & Ermopoulos ([11]-[12]) have developed a model where all the components of the connection are assumed to reach their full plastic resistance at ultimate state. Hence, the tensile components would have to be sufficiently "ductile" to permit the mobilization of all components and tube-wall buckling should be avoid.

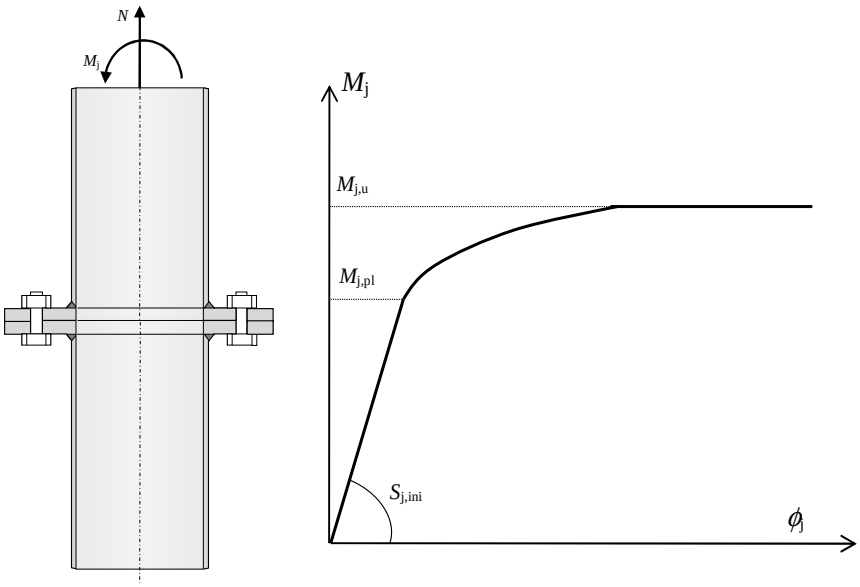


***Figure 1 :*** *Bolted circular flange joint subjected to a bending moment and an axial force*

The strength of a connection plays an important role in design. However, its stiffness can have an important impact on the overall behaviour of the structure. A model has been proposed by Kozlowski & Wojnar ([13], [14], [15]) to evaluate the initial rotational stiffness of these connections but the calculation method involves an iterative procedure and is not suitable for a day-to-day design.

The objective of this paper is to propose a new model that fully characterize the behaviour of this type of connection, and particularly the moment-rotation curve (see Figure 1). As suggested in EN 1993-1-8, the moment rotation curve is drawn based on two essential characteristics of the connection: the bending resistance and the initial rotational stiffness. The proposed model provides the static resistance of a bolted circular flange connection subjected to the full range of

combinations of bending moment and compressive or tensile axial load. This model considers two statically admissible force distributions depending on the ductility of the tensile part and the shell buckling resistance of the compressive part. The resistance of all components can be fully reached provided that they are sufficiently ductile, this mode is then called “ductile mode”. In the case of a “non-ductile mode”, the resistance of the connection is considered to be attained once the most loaded component fails. The components method is considered to determine the initial rotational stiffness. To validate this model, a bending test has been performed on a ring flange connection and completed by a parametric study considering 20 connections subjected to the combination of a bending moment and an axial force. It is shown that the proposed models predict well the initial stiffness as well as the connection resistance.

## 2. Experimental test

### 2.1. Test set-up and specimen geometry

An experimental test has been performed in the laboratory of INSA in Rennes on a bolted circular ring flange connection subjected to a bending moment. This connection, typically used in pylon of sky-lift, is composed of two forged flanges of 40 mm thickness welded on a tube 762×6 (see Figure 2). Flanges are bolted using 24 bolts HR M24 [16]. The steel grade of the tubes and the flanges is S355, and the bolts are class 10.9.

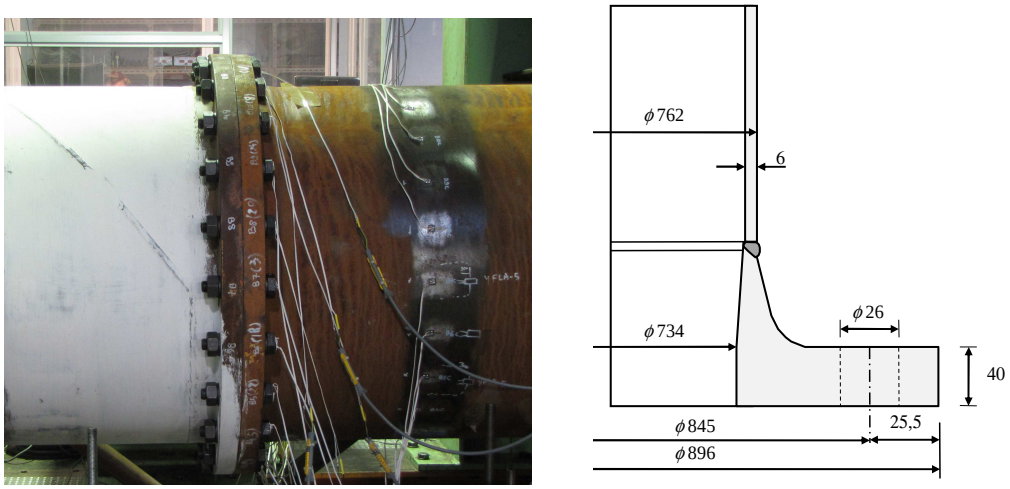


***Figure 2 :*** *Specimen tested and main dimensions (in mm)*

Figure 3 gives an overview of the four point bending flexural test set-up. The specimen comprises two tubular segments of 3,75 m connected by the bolted circular flanges. The

specimen is loaded by two load-jacks with a capacity of 1500 kN. The loading is force-controlled during the elastic stages and displacement-controlled during the elasto-plastic stage.

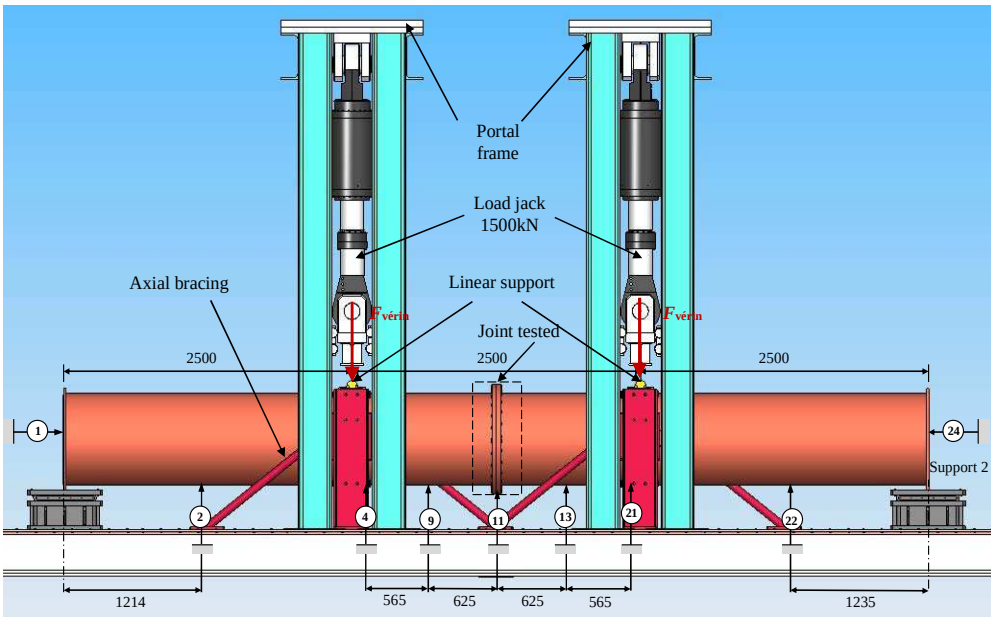


***Figure 3 :*** *Set-up of 4 points bending test (dimensions in mm)*

The connection was initially tested in the elastic range for three levels of bolt tightening: 10, 50 and 100 % of the nominal preloading according to EN 1090-2 [17] with the aim to evaluate the effect of preloading on the bolt forces distribution. The nominal preloading forces are increased by 10 % as required by the torque method (see Table 1). Half of the bolts were instrumented (see Figure 5). For these bolts, tightening was performed by reading the strain gauge according to the calibration factor. Non-instrumented bolts were tightened applying the torque method of EN 1090-2 [17]. During these stages, the magnitude of the bending moment was selected to avoid any yielding for each level of preloading. These three cycles are named stage 1, 2 and 3 respectively.

| $B_0$ (kN) | | | Bolt |
|---|---|---|---|
| Stage 1 | Stage 2 | Stage 3 | |
| 27 | 135 | 270 | M24 |

***Table 1 :*** *Bolt preloading force*

After these three elastic cycles, HR bolts were preloaded to 20 % of the nominal preloading as specified in EN 1090-2. The specimen was loaded until failure of the connections so as to

evaluate the elasto-plastic behaviour and particularly the plastic and ultimate resistances. This step corresponds to stage 4.

### *2.2. Initial imperfections of the flanges*

Near each bolt, the position of the flanges has been measured at the outer edge (point 2 in Figure 4) and at the inner edge of the flanges (point 1 in Figure 4). The difference between these two points corresponds to the imperfection of the flange:

$$\Delta = \text{Position}2 - \text{Position}1 \tag{1}$$

The mean value of initial flange imperfection [18] is equal to 1,09 mm and tends to favour contact at the outer edge of the flanges as indicated in Figure 4.

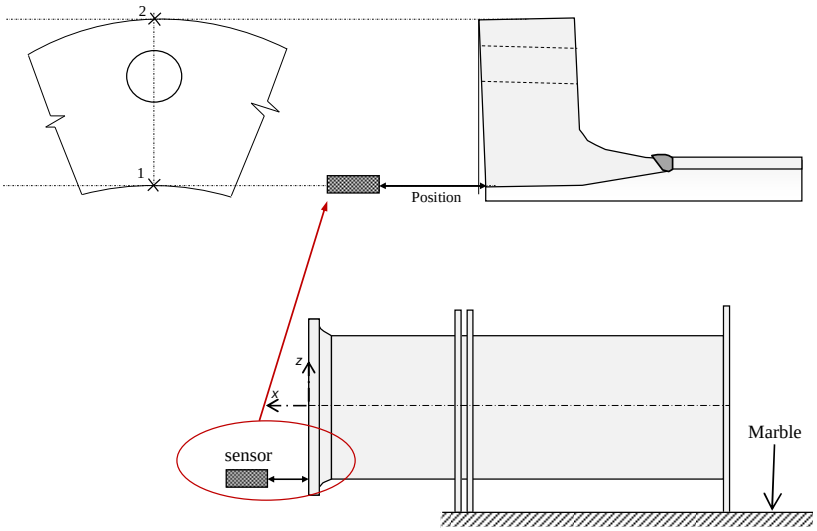


***Figure 4 :*** *Measurement of the initial imperfections of the flanges*

### *2.3. Measurements*

During the test, bolt forces, displacements and strains in the connection were measured. Two rosette strain gauges (BR1 and BR2) have been placed on the flange to measure radial and hoop strains (see Figure 5). Two rosette strain gauges (TR1 and TR2) have also been positioned on the tube at 15 mm of the weld toe for the same reason. Thirteen axial strain gauges located at 300 mm of the weld toe have been used to estimate the axial strain distribution in the tube. Thirteen bolts have been instrumented with axial strain gauges BTM-6C in order to measure the axial strain and thus by calibration, the tensile force in the bolts. Instrumented bolts have also been used to control the bolt preload during tightening as explained in section 2.1. The main

displacement transducers (LVDT) positioned to measure the displacements at different locations on the test specimen are presented in Figure 3.

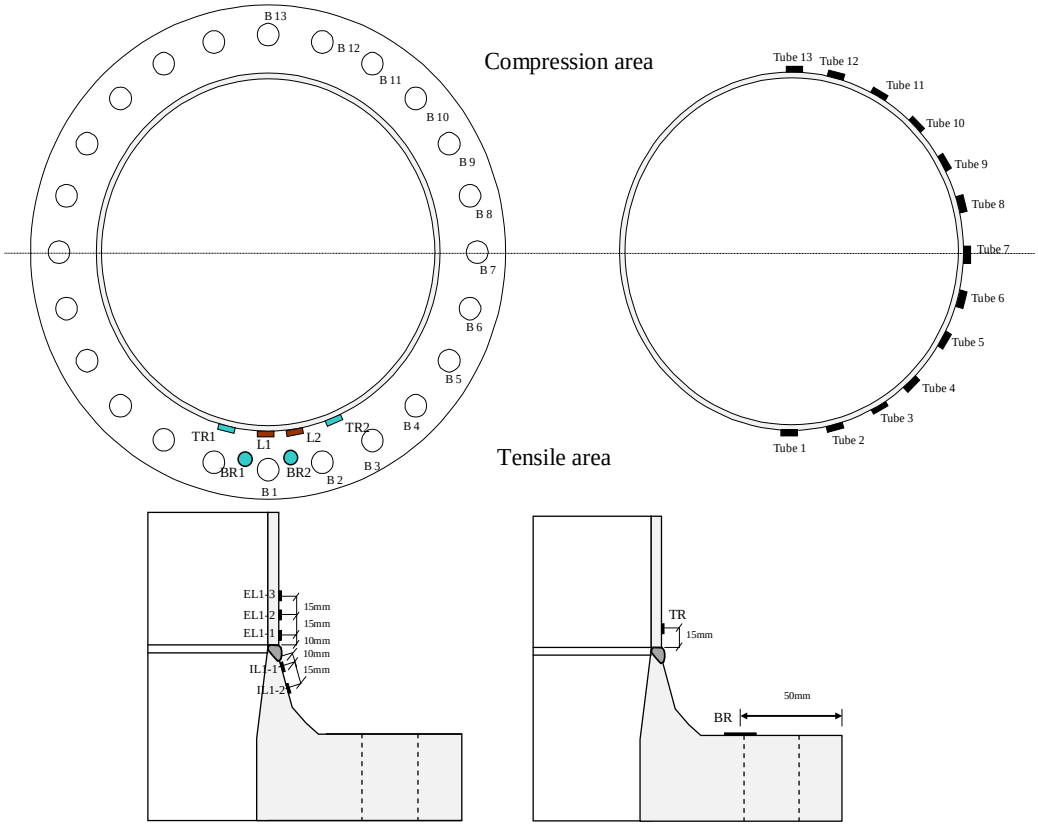


***Figure 5 :*** *Strain gauges on the flange and on the tube-wall*

### *2.4. Mechanical characteristics of steel*

Coupons extracted from the tube and the flanges as well as the bolts have been tested according to NF EN 10002-1. The mean value of mechanical characteristics of the bolts, the flanges and the tubes are given in Table 2.

| Component | Thickness/ length | Module of elasticity | Yield strength | Tensile strength | Elongation | Necking |
|---|---|---|---|---|---|---|
| | *mm* | *N/mm²* | *N/mm²* | *N/mm²* | *%* | *%* |
| Tube | 6 | 215717 | 351 | 492 | 16,2 | 60 |
| Flange | 40 | 214419 | 328 | 529 | 16 | 73 |
| Bolts | 120 | 212792 | 1110 | 1156 | 21 | 59 |

***Table 2 :*** *Mechanical characteristics of tubes, flanges and bolts*

### *2.5. Test results*

#### *2.5.1. Moment-rotation curve*

Failure of the specimen occurred by local tube-wall buckling at the junction with the connections just above the weld (see Figure 6). It was observed that the three most tension-

loaded bolts yielded just prior the end of the test (see section 2.5.2). The maximum bending moment resisted by the connection during the test is equal to 925 kNm.

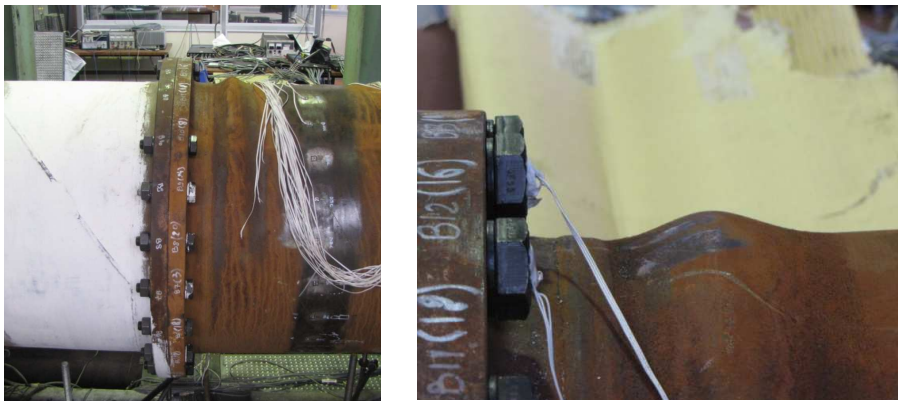

***Figure 6 :*** *Specimen after local buckling*

The connection rotation has been evaluated using the displacement given by transducer n°21 (see Figure 3):

$$\phi_j = 2.\frac{\delta_{21,\text{measured}} - \delta_{21,\text{theoretical}}}{L_{21}} \tag{2}$$

where $\delta_{21,\text{merasured}}$ is the displacement measured by LVDT n°21 (see Figure 3), $\delta_{21,\text{theoretical}}$ the theoretical displacement calculated at the location of LVDT n°21 and $L_{21}$ the distance from LVDT n°21 to support n°2.

The moment-rotation curve is depicted in Figure 7 for stage 4. The elastic stage is rapidly followed by a drop of the bending moment. This is a typical situation observed with shell-type local buckling behaviour.

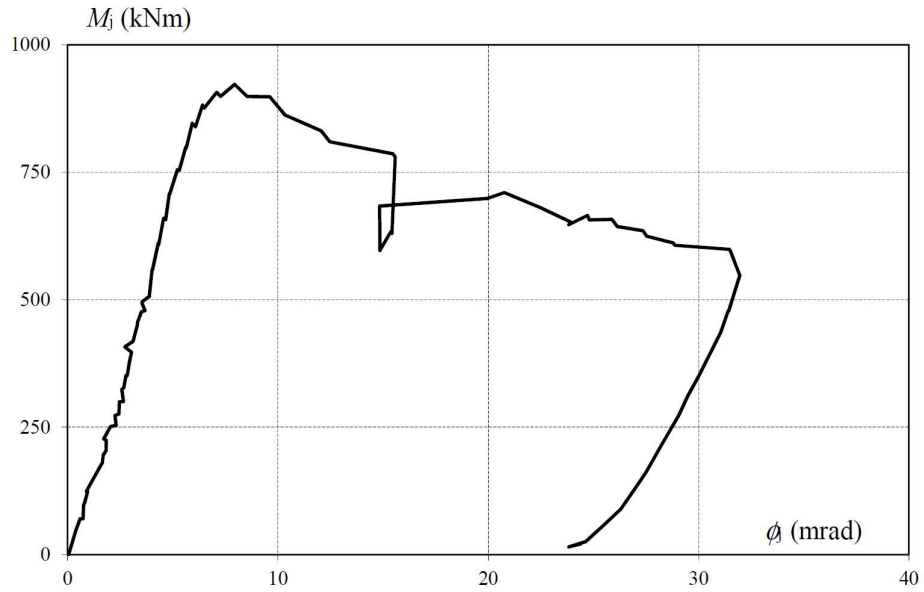


***Figure 7 :*** *Moment rotation curve – experimental test*

### *2.5.2. Bolt forces*

The relationships between the force in bolt n°1 and the bending moment in the connection during the four stages is presented in Figure 8. During stages 1, 2 and 4 the variation of the bolt force is almost linear in contrast with what happens during stage 3 where 110 % of nominal preloading according to EN 1090-2 is applied. Effect of preloading on the variation of the bolt force is irrelevant during phases 1, 2 and 4 mainly due to the initial imperfections (see section 2.2). At the end of stage 4, bolt n°1 yields in tension.

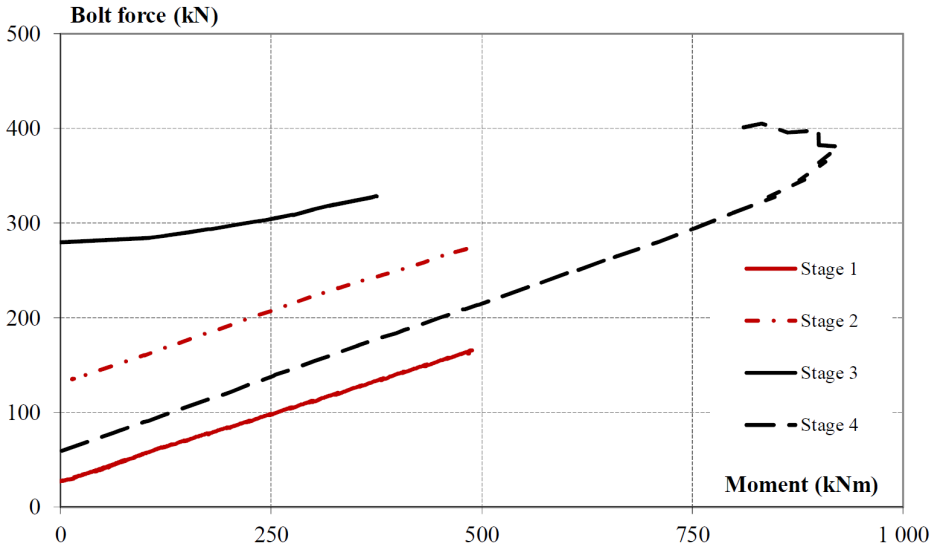


***Figure 8 :*** *Evolution of bolt force n°1 – experimental test*

The distribution of the bolt forces for different values of the bending moment applied to the connection in function of their location relatively to the mid-axis of the tube is presented in Figure 9. For bolts located in the compressive area, a decrease of the bolt force is observed due to the transverse local deformation of the flange. An increase of the bolt force is obtained in the tensile area that is lower during stage 3 than stage 4. For large values of the bending moment, the distribution of the bolt forces in the tensile zone is almost linear during stage 4. A mildly non-linear response of bolt forces can be observed as consequence of bolt preloading (see Figure 8). A plastic redistribution of bolt forces was not possible due to the local buckling of the tube that appears just after yielding of three bolts in the tensile area.

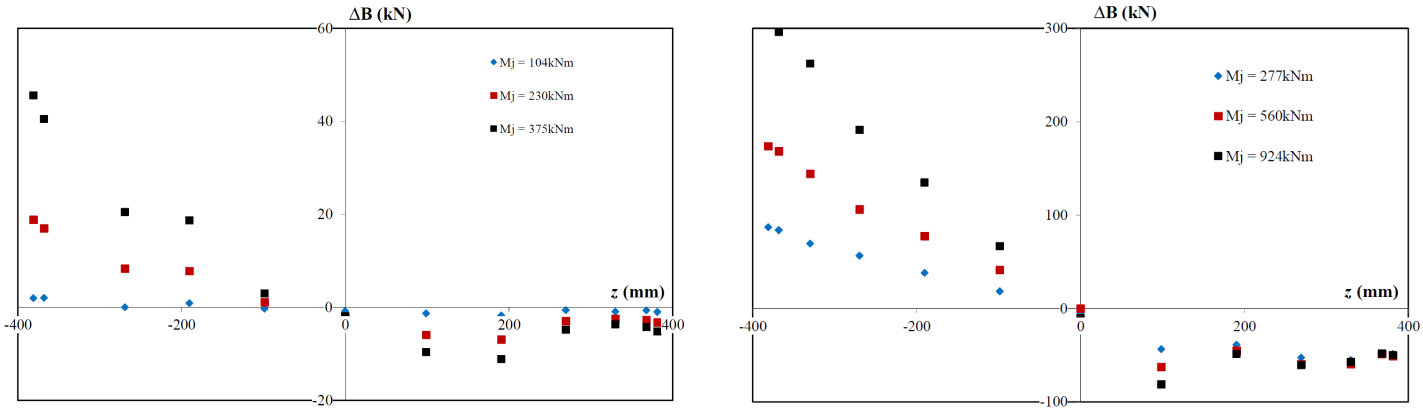


*a- Stage 3* *b- Stage 4*

***Figure 9 :*** *Variation of bolt forces – experimental test*

### *2.5.3. Strain gauge measurements*

Rosette strain gauges BR1 and BR2 show that at failure the flanges remain elastic in the tensile area. The elongations of bolts was not sufficient in the tensile area to lead to a cambering of the flanges as it was observed for the bolted circular flange connections subjected to a tensile force tested by Couchaux et al [4]. Stresses calculated with strains measured by axial gauges placed at 300 mm of the connections Tube $i$ $(i = 1 \rightarrow 13)$ are presented in Figure 10.

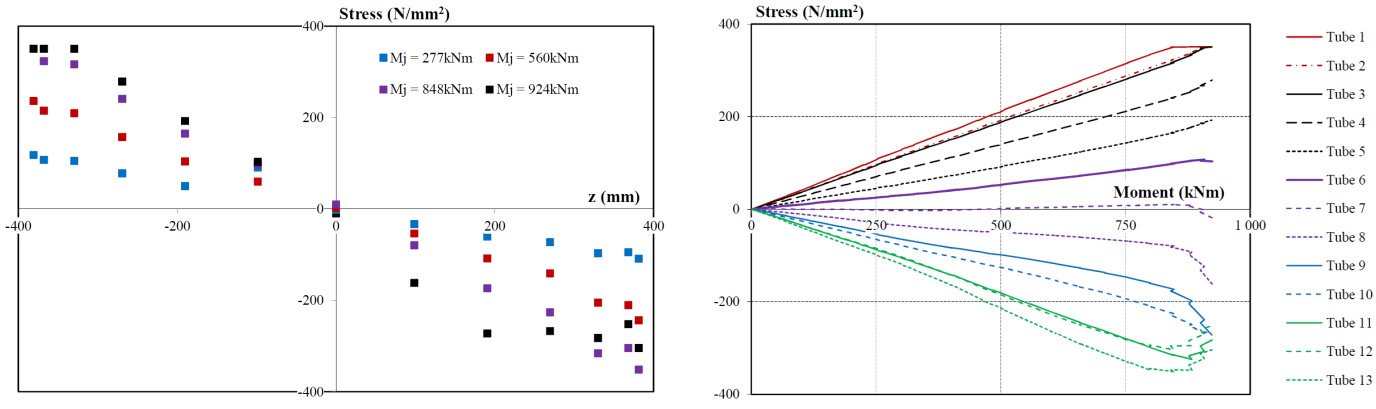


*a- Distribution of stresses* *b- Evolution of stresses*

***Figure 10 :*** *Axial stresses on the tube during stage 4*

The evolution of stresses as a function of bending moment is linear until the development of stresses close to the yield strength in the tensile and compressive areas for a bending moment close to 850 kNm. Then, the stresses decrease in the most compressed strain gauges (Tube 11, 12 and 13) and increase in the remaining strain gauges placed in the compression area. This redistribution of stresses is caused by the local buckling of the tube-wall in the vicinity of the connection. At the end of the test, strain gauges Tube 1, 2 and 3 reach the yield stress. The tube was able to develop its elastic bending moment.

## *3. Numerical analysis*

### *3.1. Presentation of the finite element model*

A numerical model has been developed to carry out a parametric study and to complete the available experimental results ([19], [20], [21], [22]). The numerical model was built using the Finite element code ANSYS V11.0. This model is quite similar to that developed for bolted

circular flange connections subjected to a tensile force [4]. Connections are generated with 3D solid elements (hexahedral or tetrahedral bricks). The bolts are modelled considering a constant cross-section equal to the effective area $A_s$ specified by EN1993-1-8. The model domain consists of 1/4 of the full geometry, since there are two planes of symmetry (see Figure 11).

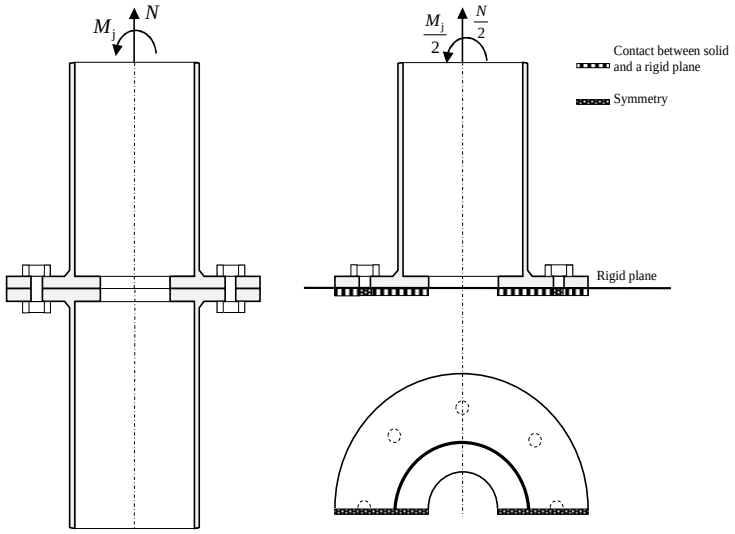


***Figure 11 :*** *Symmetries of the model and contact elements*

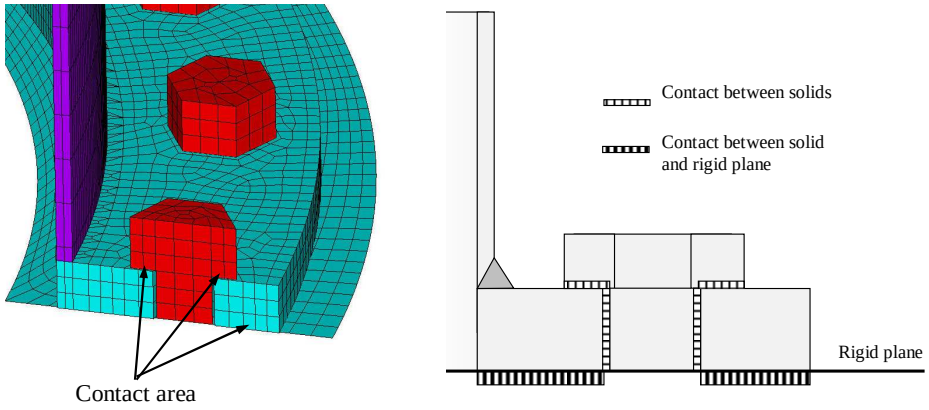


***Figure 12 :*** *Contact areas*

Contact elements are used between the flange and the bolts, and rigid contact elements between one flange and the horizontal plane of symmetry. An isotropic Coulomb friction law ($\mu$ = 0,25) is used to reproduce sliding/sticking conditions between the flange and the bolt. Friction is neglected between the two flanges because of the symmetry.

The stress-strain relationship for steel (flange, tube and bolts) is assumed to be multi-linear (see Figure 13). Large deformations are also considered. As soon as the deformation level reaches $\varepsilon_u$, the stress drops to 10 N/mm$^2$ in order to model the failure of the element. This

phenomenon leads either to a drop-off of the force applied to the connection or to the termination of the calculation. This latter state is assumed to be the ultimate state for the connection. The Von Mises criterion is retained to monitor plastic yielding. A complete curve has been used for the analysis of the tested specimen and considers true stress and true strain. For the parametric study, a simple bi-linear curve has been used (see Figure 13-b). The true stress-strain curve was built considering ($f_y$, $\varepsilon_y$), ($f_y$, $\varepsilon_h$), ($f_m$, $\varepsilon_m$) and ($f_u$, $\varepsilon_u$) that were determined from coupon test results (see section 2.4 and Couchaux et al [7]).

The extremity of the tube is linked to a pilot node where rotation or bending moment are applied. Loading is controlled in rotation for pure bending moment in order to be able to observe the post-critical regime. In the case of combined loading, the normal force (force controlled loading) is firstly applied. Next the rotation of the pilot node is progressively increased.

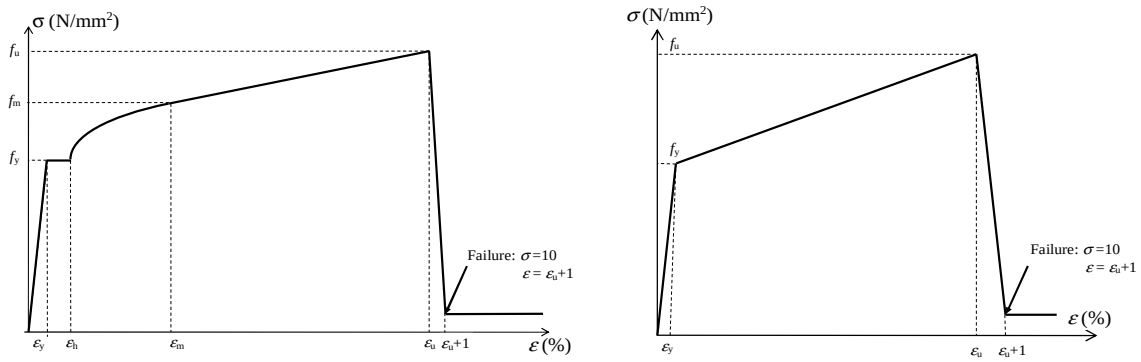


*a- Complete curve* *b- Simplified curve*

***Figure 13 :*** *Stress-strain curves*

## *3.2. Comparison to test results*

### *3.2.1. Geometrical and mechanical characteristics*

A quarter of the connection is modelled as explained in the previous section and presented in Figure 14. The length of the tube is equal to 1250 mm. Analyses have been performed considering four levels of bolt preloading:

- Stage NP: Bolts are not preloaded and a bending moment equal to 400 kNm is applied,
- Stage 2: Bolts are preloaded to half the nominal preloading of EN 1090-2 and a bending moment equal to 580 kNm is applied,

- Stage 3: Bolts are preloaded to the complete nominal preloading of EN 1090-2 and a bending moment equal to 360 kNm is applied,
- Stage 4: Bolts are preloaded to 20 % of the nominal preloading of EN 1090-2 and the rotation is increased until post-buckling.

A geometrical imperfection homothetic to the buckling mode shape obtained at failure (see Figure 15) was applied with a magnitude equal to 1,4 mm.

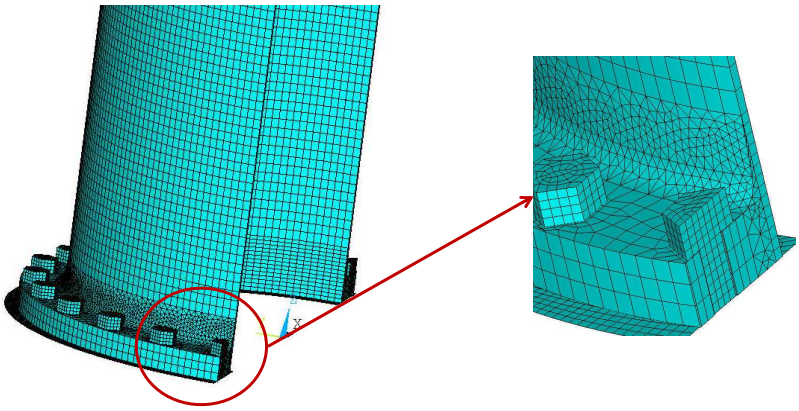

***Figure 14 :*** *Finite element mesh*

The mechanical properties used with the strain-stress curve presented in Figure 13-a are given in Table 3.

| Element | Thickness/ Diameter | $E$ | $f_y$ | $\varepsilon_h$ | $f_m$ | $\varepsilon_m$ | $f_u$ | $\varepsilon_u$ |
|---|---|---|---|---|---|---|---|---|
| | | $N/mm^2$ | $N/mm^2$ | % | $N/mm^2$ | % | $N/mm^2$ | % |
| tube | 6 | 215717 | 352 | 2,00 | 578 | 16,1 | 940 | 90,9 |
| flange | 40 | 214419 | 329 | 1,33 | 621 | 16,0 | 1230 | 130,9 |
| bolt | 24 | 210154 | 1122 | 0,56 | 1264 | 4,40 | 1402 | 89 |

**Table 3 :** *Mechanical characteristics used to model experimental test*

*3.2.2. Moment rotation curves*

The failure mode obtained with the finite element model corresponds to local buckling of the tube at the junction with the flange (see Figure 15-b). Most tension-loaded bolts yield before the maximum bending moment is reached. The ultimate bending moment obtained numerically is equal to 911 kNm and close to the measured ultimate bending moment equal to 925 kNm.

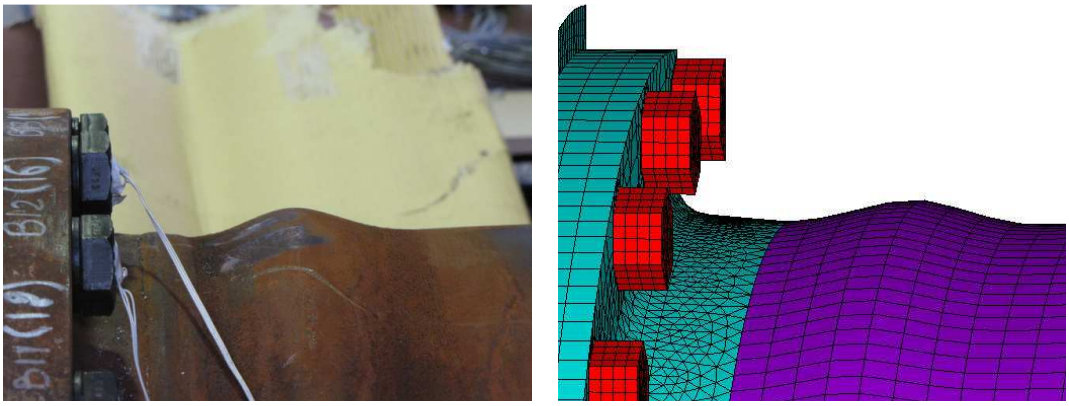

*a- Test* *b- Numerical*

***Figure 15 :*** *Local buckling of the tube-wall*

The moment-rotation curves of the connection obtained numerically and experimentally during stage 4 are depicted in Figure 16. Overall a fairly good match is observed as the global behaviour is well reproduced. The stiffness in the elastic domain is very well estimated, however the decrease of the bending moment occurring after tube buckling is more progressive and regular (constant slope).

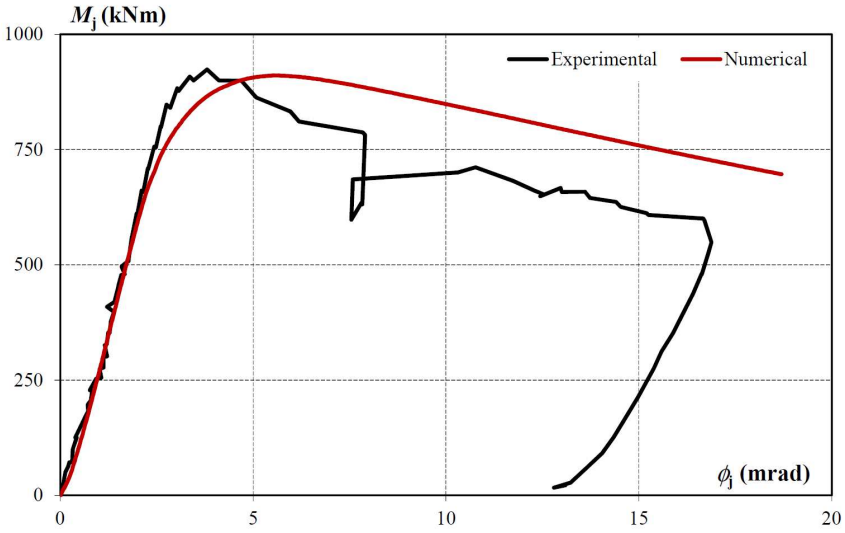


***Figure 16 :*** *Moment rotation curve*

### *3.2.3. Bolt forces*

The evolution of the bolt forces during phases 2, 3 and 4 is presented in Figure 17 as a function of the bending moment. During stage 4, the evolution of the bolt forces is clearly linear until the bending moment reaches 900 kNm. During stages 2 and 3, the variation of bolt forces is more progressive at the beginning of loading than at the end due to the effect of bolt preloading. This phenomenon also happens in L-stub and bolted circular flange in tension ([4],

[7]). At the beginning of loading, the contact area is located behind the bolts (see Figure 18-a) and the bolt elongation, and thus the bolt tensile force, is limited. The bolt forces further increase after partial uplift of the flanges occurs (see Figure 18-b).

The evolution of the force in the most tension-loaded bolt (in fact bolt n°1) is presented in Figure 19 as a function of the bending moment applied to the connection during stages 2, 3 and 4. The increase of bolt forces is more important in the test than in the numerical model. This difference is mainly due to the initial deformed shape of flanges (see section 2.2) that improves the contact at the outer edge of flanges. Effect of preloading decreases with increasing value of the applied load. As a result, the variation of bolt force is more pronounced. These phenomena were highlighted by Jakubowski & Schmidt [20].

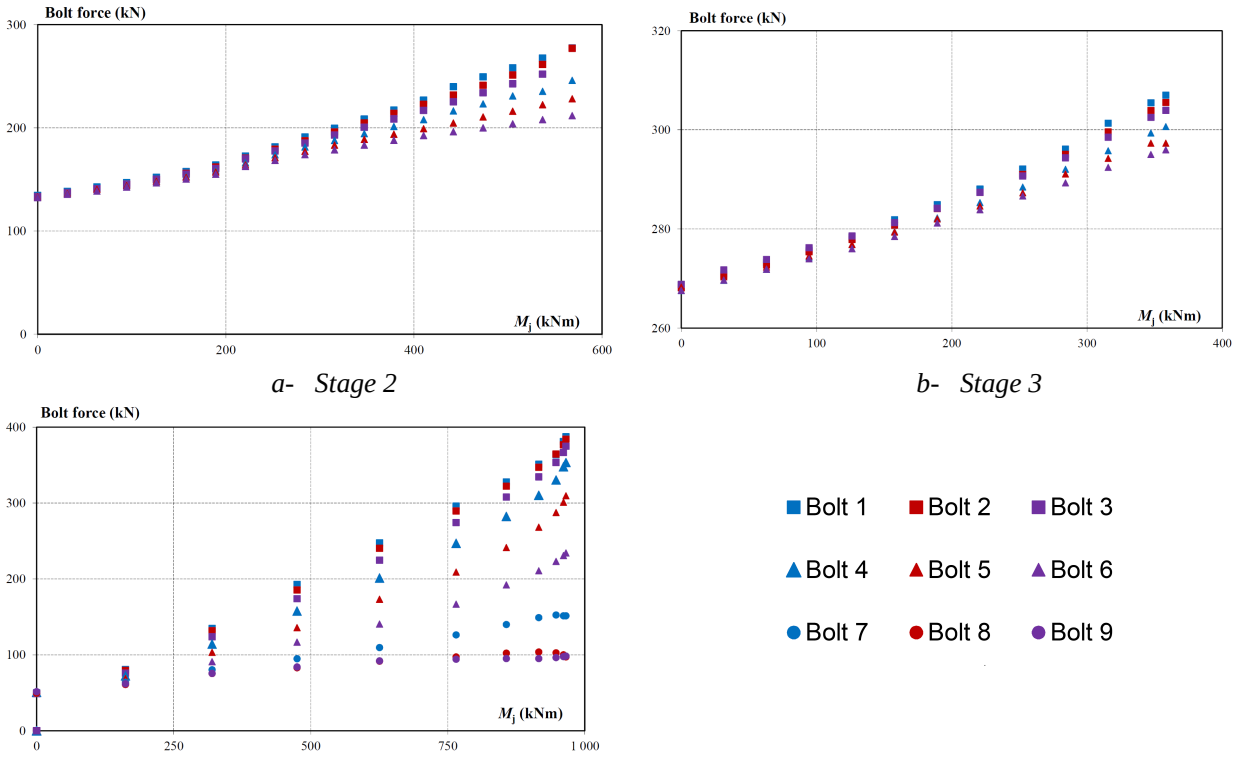


*a- Stage 2*

*b- Stage 3*

*c- Stage 4*

***Figure 17 :*** *Evolution of bolt forces*

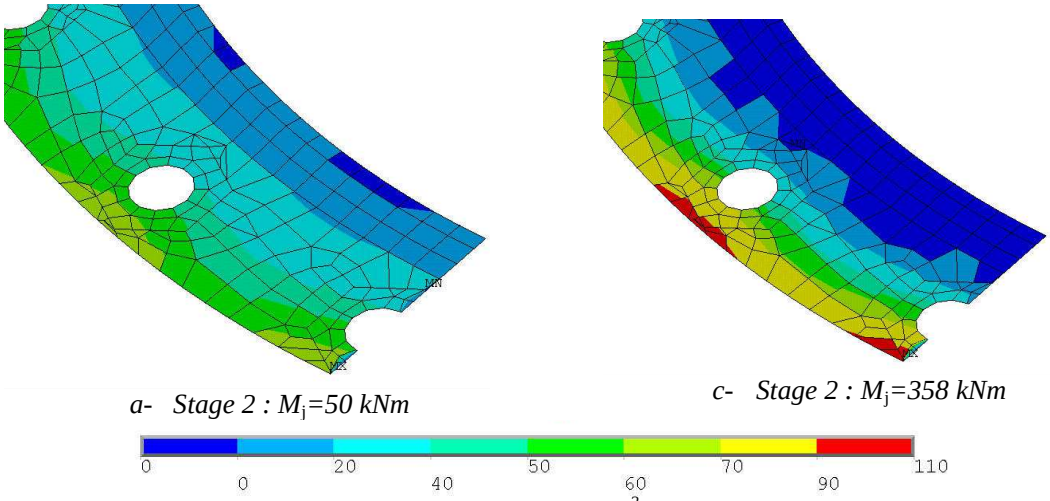


*a- Stage 2 : $M_j$=50 kNm*

*c- Stage 2 : $M_j$=358 kNm*

***Figure 18 :*** *Contact stress (in N/mm$^2$) in the tensile area*

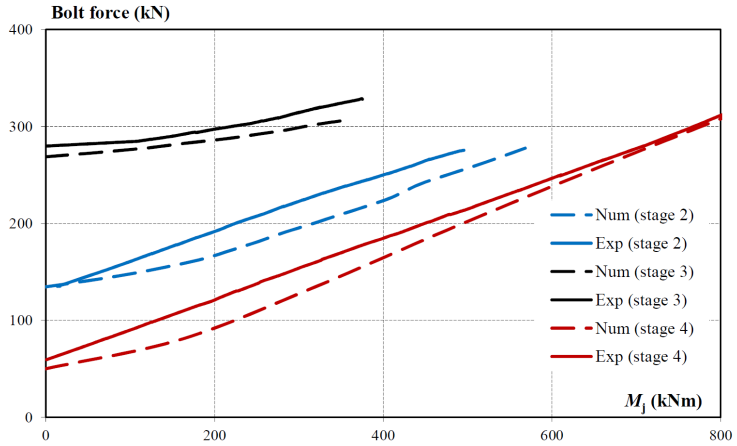


***Figure 19 :*** *Evolution of bolt force n°1*

### *3.3. Parametric study*

#### *3.3.1. Dimensions of specimens*

A parametric study has been performed considering 20 bolted circular flange connections (see Table 4 and Figure 20) subjected to either a pure bending moment or to a combination of bending moment and axial force (compression or tension). Specimens M15 to M19 are made of blank flanges whilst the remaining specimens are ring flanges. Bolts were not preloaded.

| Specimen | $R_f$ | $R_b$ | $R_0$ | $t_f$ | $R$ | $t_t$ | $L_1$ | Bolt | $n_b$ |
|---|---|---|---|---|---|---|---|---|---|
| | *mm* | *mm* | *mm* | *mm* | *mm* | *mm* | *mm* | mm | - |
| M1 | 459 | 423 | 368,5 | 40 | 374,75 | 12,5 | 1500 | 24 | 24 |
| M2 | 526 | 463 | 365 | 40 | 373 | 16 | 1500 | 24 | 24 |
| M3 | 459 | 423 | 368,5 | 20 | 374,75 | 12,5 | 1500 | 24 | 24 |
| M4 | 459 | 423 | 368,5 | 15 | 374,75 | 12,5 | 1500 | 24 | 24 |
| M5 | 459 | 423 | 375 | 40 | 378 | 6 | 1500 | 24 | 24 |
| M6 | 459 | 423 | 375 | 20 | 378 | 6 | 1500 | 24 | 24 |
| M7 | 459 | 423 | 375 | 20 | 378 | 6 | 1500 | 24 | 24 |
| M8 | 395 | 350 | 300 | 10 | 302,5 | 5 | 900 | 20 | 24 |
| M9 | 395 | 350 | 300 | 15 | 302,5 | 5 | 900 | 20 | 24 |
| M10 | 395 | 350 | 300 | 25 | 302,5 | 5 | 900 | 20 | 24 |
| M11 | 395 | 350 | 300 | 40 | 302,5 | 5 | 900 | 20 | 24 |
| M12 | 620 | 560 | 502 | 40 | 508 | 12 | 1000 | 30 | 24 |
| M13 | 620 | 560 | 502 | 30 | 508 | 12 | 1000 | 30 | 24 |
| M14 | 620 | 560 | 502 | 20 | 508 | 12 | 1000 | 30 | 24 |
| M15 | 155 | 132 | 0 | 10 | 97,75 | 4,5 | 250 | 16 | 8 |
| M16 | 155 | 132 | 0 | 20 | 97,75 | 4,5 | 250 | 16 | 8 |
| M17 | 155 | 132 | 0 | 20 | 96 | 8 | 500 | 16 | 8 |
| M18 | 160 | 120 | 0 | 20 | 80,15 | 8 | 400 | 16 | 8 |
| M19 | 160 | 120 | 0 | 15 | 80,15 | 8 | 300 | 16 | 8 |
| M20 | 160 | 120 | 76,15 | 15 | 80,15 | 8 | 300 | 16 | 8 |

$n_b$ : Number of bolts

***Table 4 :*** *Geometry of connections – parametric study*

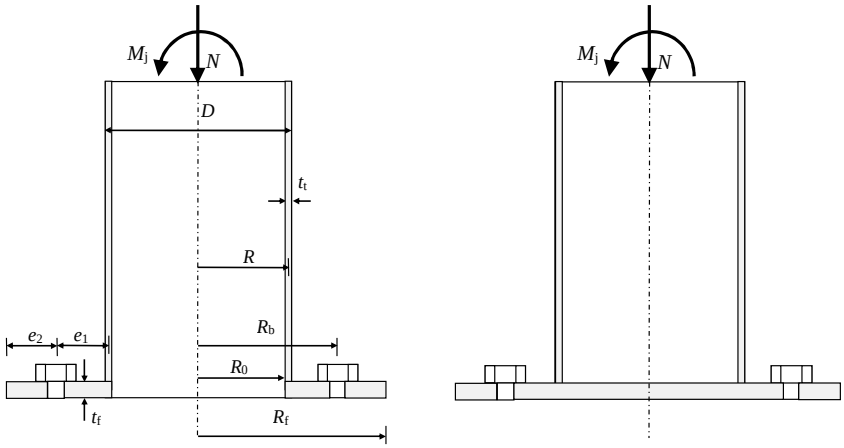


*a- Ring flange* *b- Blank flange*

***Figure 20 :*** *Dimensions of specimens studied*

The objective of this parametric study is to quantify the effect of the flange and tube thicknesses as well as the diameter of the tube. The behaviour of steel is multilinear as described in Figure 13-b and mechanical characteristics are given in Table 5.

| Specimen | Flange | | | Tube | | | Bolt | | |
|---|---|---|---|---|---|---|---|---|---|
| | $f_{y,f}$ | $f_{u,f}$ | $\varepsilon_{u,f}$ | $f_{y,t}$ | $f_{u,t}$ | $\varepsilon_{u,t}$ | $f_{y,b}$ | $f_{u,b}$ | $\varepsilon_{u,b}$ |
| | $N/mm^2$ | $N/mm^2$ | % | $N/mm^2$ | $N/mm^2$ | % | $N/mm^2$ | $N/mm^2$ | % |
| M1 | 355 | 637 | 30 | 355 | 637 | 30 | 900 | 1100 | 10 |
| M2 | 235 | 468 | 30 | 235 | 468 | 30 | 900 | 1100 | 10 |
| M3-M6 | 355 | 637 | 30 | 355 | 637 | 30 | 900 | 1100 | 10 |
| M7 | 355 | 637 | 30 | 355 | 637 | 30 | 640 | 880 | 10 |
| M8-M14 | 355 | 637 | 30 | 355 | 637 | 30 | 900 | 1100 | 10 |
| M15-M17 | 355 | 637 | 30 | 355 | 637 | 30 | 640 | 880 | 10 |
| M18-M20 | 355 | 637 | 30 | 460 | 702 | 30 | 640 | 880 | 10 |

***Table 5 :*** *Mechanical characteristics – parametric study*

### *3.3.2. Failure modes*

Failure modes, plastic and ultimate bending moments, along with yielded components at failure are reported in Table 6.

| Specimen | $N$ | $M_{j,pl}$ | $M_{j,u}$ | $M_{j,u}/M_{j,pl}$ | Yielded components | Failure |
|---|---|---|---|---|---|---|
| | *kN* | *kNm* | *kNm* | - | | |
| M1 | 0 | 1469 | 1809 | 1,23 | Bolt | Bolt |
| M2 | 0 | 1284 | 1524 | 1,19 | Bolt | Bolt |
| M3 | 0 | 1158 | 1529 | 1,32 | Bolt | Bolt |
| M4 | 0 | 905 | 1581 | 1,75 | Bolt-tube | Bolt |
| M5 | 0 | 990 | 1079 | 1,09 | Bolt, tube | Buckling |
| M6 | 0 | 833 | 943 | 1,13 | Flange, bolt, tube | Buckling |
| M7 | 0 | 746 | 882 | 1,18 | bolt, tube | Buckling |
| M8 | 0 | 196 | 313 | 1,60 | Flange, tube | Buckling |
| M9 | 0 | 336 | 413 | 1,23 | Flange, tube | Buckling |
| M9-N=-0,5MN | -500 | 249 | 424 | 1,70 | Flange, tube | Buckling |
| M9-N=-1MN | -1000 | 227 | 456 | 2,01 | Flange, tube | Buckling |
| M9-N=-1,5MN | -1500 | - | 372 | - | Flange, tube | Buckling |
| M9-N=0,5MN | 500 | 405 | 424 | 1,05 | Flange, tube | Buckling |
| M9-N=1MN | 1000 | 162 | 412 | 2,55 | Tube | Buckling |
| M10 | 0 | 523 | 561 | 1,07 | Bolt, tube | Buckling |
| M10-N=-1MN | -1000 | 406 | 541 | 1,33 | Bolt, tube | Bolt |
| M10-N=-2MN | -2000 | 226 | 312 | 1,38 | Bolt | Bolt |
| M10-N=1MN | 1000 | 406 | 457 | 1,13 | Tube | Buckling |
| M10-N=2MN | 2000 | 281 | 307 | 1,09 | Tube | Buckling |
| M11 | 0 | 568 | 590 | 1,04 | Tube | Buckling |
| M12 | 0 | 2784 | 3402 | 1,22 | Bolt | Bolt |
| M13 | 0 | 2732 | 3249 | 1,19 | Bolt | Bolt |
| M14 | 0 | 2122 | 2917 | 1,37 | Bolt, flange, tube | Bolt |
| M15 | 0 | 39 | 49 | 1,25 | Bolt, flange, tube | Bolt |
| M16 | 0 | 59 | 60 | 1,03 | bolt, tube | Buckling |
| M17 | 0 | 71 | 85 | 1,20 | Bolt | Bolt |
| M18 | 0 | 64 | 78 | 1,22 | Bolt-flange-tube | Bolt |
| M19 | 0 | 51 | 64 | 1,26 | Bolt | Bolt |
| M20 | 0 | 42 | 54 | 1,27 | Bolt | Bolt |

***Table 6 :*** *Failure modes – parametric study*

The plastic bending moment $M_{j,pl}$ is estimated according to the ECCS method via the moment-rotation curve [23]. When bolts and/or flanges yield in the tensile part, a yield line develops within the tube wall just above the junction with the flange. Failure corresponds either to bolt rupture in tension (Figure 21-b) or to buckling of the tube wall above the compressed part of the flange (Figure 21-a). For a large number of specimens, buckling of the tube-wall is preceded by important yielding of the tensile part of the connection (bolts and/or flanges).

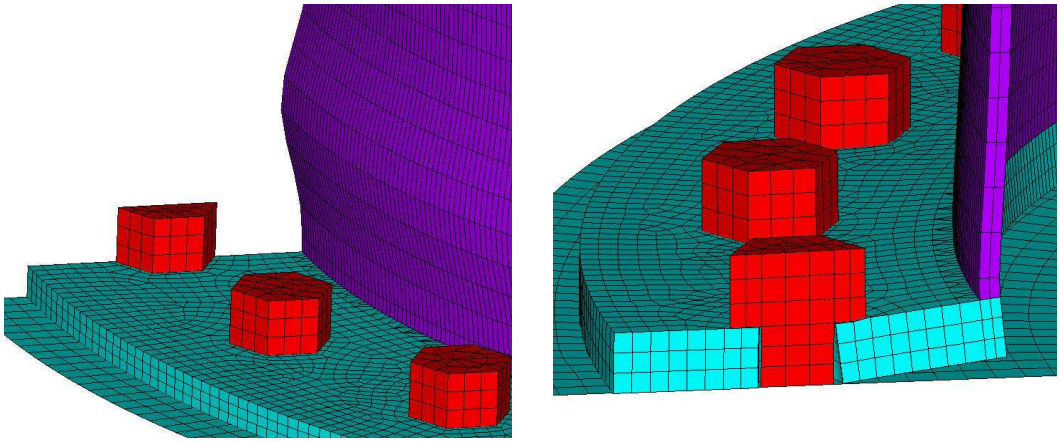

*a- Local buckling of the tube wall* *b- Bolt rupture in tension*

***Figure 21 :*** *Failure mode*

*3.3.3. Influence of flange thickness*

The geometrical characteristics of specimens M8, M9, M10 and N11 are identical except the flange thickness which is equal to 10, 15, 25 and 40 mm, respectively. The moment-rotation curves for these specimens are presented in Figure 22-a. An increase of flange thickness leads to an increase of initial rotational stiffness, plastic and ultimate bending moments and a decrease of the rotation capacity. The resistance is also limited by the local buckling of the tube wall for the four specimens even if yielding of flange and bolts are obtained. For specimen M8, the rotation capacity is clearly improved due to yielding of the flanges in bending, however the buckling of the tube is finally obtained in the compressive area.

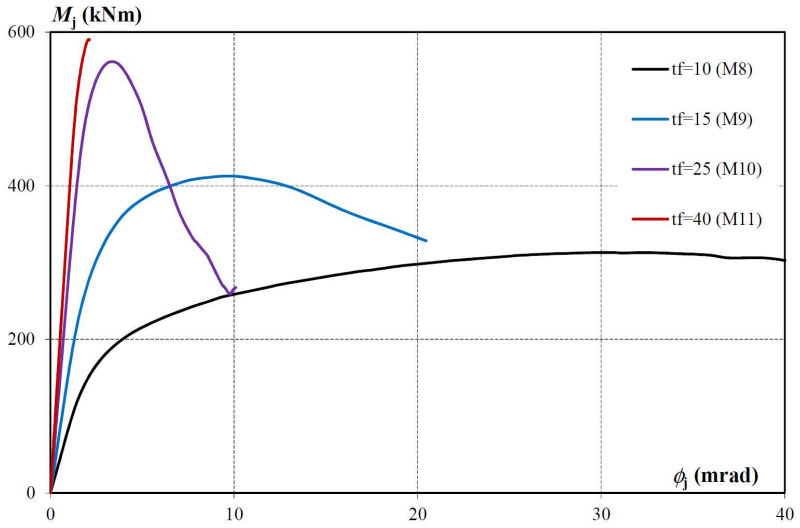


*a- Specimens N8 to N11*

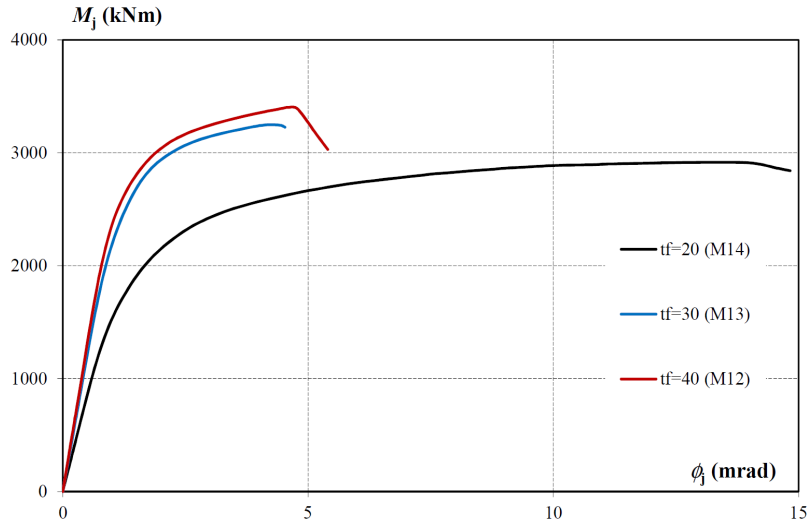


*b- Specimens N12 to N14*

***Figure 22 :*** *Moment rotation curves : Effect of flange thickness*

Similarly, the only difference between specimens M12, M13 and M14 is the flange thickness which is equal to 40, 30 and 20 mm, respectively. The moment-rotation curves for specimens M12, M13 and M14 are depicted in Figure 22-b. It has been observed that for these three specimens failure is due to bolts fracture. Furthermore, a reduction of flange thickness clearly increase the rotation capacity of the connections due to the development of plastic yield lines on the flange.

### *3.3.4. Influence of axial force*

The moment-rotation curves of specimen M9 and M10 obtained for different values of the axial force are presented in Figure 23. Compressive force increases the initial rotational stiffness whilst tensile force produces the opposite effect. The compressed area is stiffer than the tensile zone. By increasing this area, the stiffness of the connection is increased. In presence of an initial tensile force, a decrease of the stiffness is observed (particularly for specimen M10) with increasing values of the bending moment. Similarly, the stiffness decreases with increasing values of the bending moment in presence of an initial compressive force. This effect results from the development of a compression area that is stiffer than the tensile area.

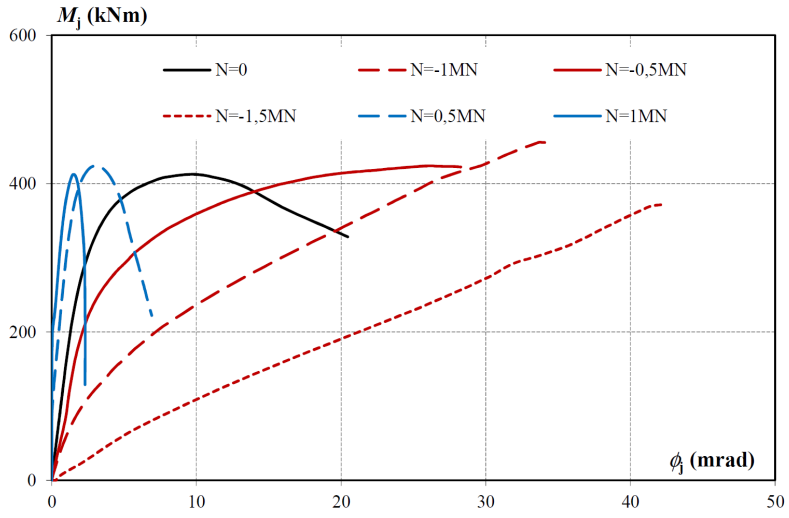


*a- Specimen M9*

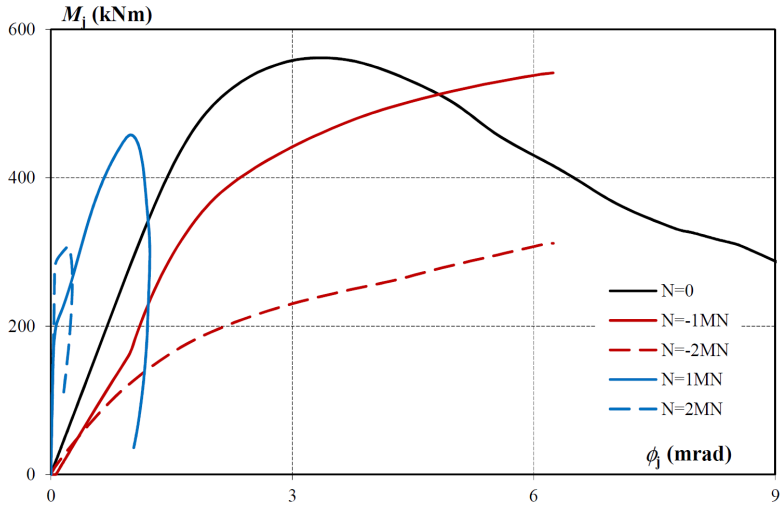


*b- Specimen M10*

***Figure 23 :*** *Moment rotation curves : Effect of axial force*

### *3.3.5. Bolt force distribution at failure*

It has been observed during test (see section 2.5.2) that, when reaching the ultimate moment, the distribution of bolt force was almost linear in the tensile area of the connection. So, the tube wall buckling occurred just after yielding of the first three bolts preventing yielding of other bolts. On the contrary, some specimens studied numerically have been able to develop important rotation capacity with most of the bolts located in the tensile area yielding before the complete failure of the connection. For instance, Specimen M12 belongs to this latter category. The evolution of the bolt forces obtained for specimen M12 is presented in Figure 24 as a function of the bending moment. The yield tensile force is reached for half the bolts of the connection at failure.

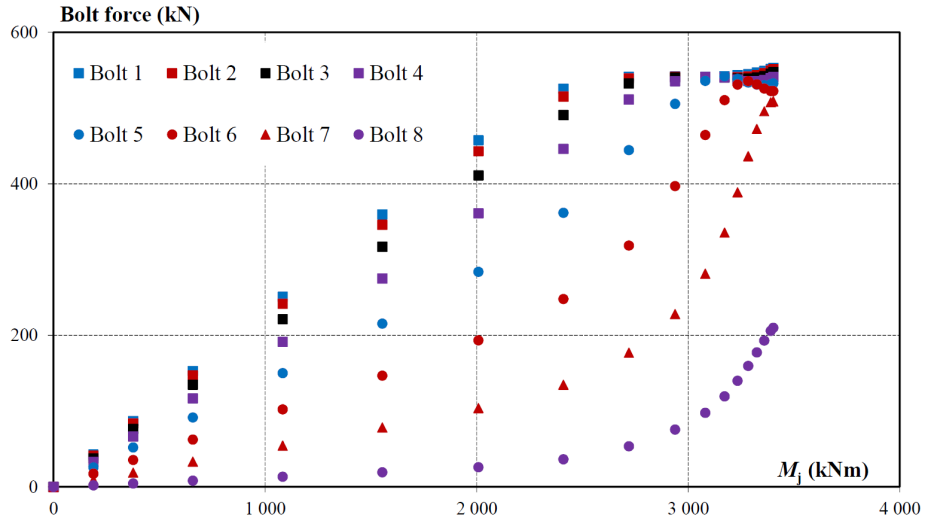


***Figure 24 :*** *Evolution of bolt forces : Specimen M12, N = 0*

## *4. Analytical model for moment-rotation curve*

### *4.1. Introduction*

The objective of this section is to propose a model which fully characterize the behaviour of this type of connections, and particularly the moment-rotation curve. As suggested in EN 1993-1-8, the moment rotation curve is built on two essential characteristics of the connection: the static bending resistance and the initial rotational stiffness. The static bending resistance of connection is evaluated considering either a fully plastic mechanism or a deformation mode where only part of the connection is plasticized (see section 4.3). The initial rotational stiffness

is determined in section 4.2 considering the component method. The tensile part is modelled considering an L-stub in tension [24]. Based on the model developed by Couchaux et al [25] for beams in contact with a rigid foundation, a new component, corresponding to flanges in compression, is derived and used to determine the position of the neutral axis of the connection. The results obtained via this analytical model are compared favourably against numerical predictions and experimental results.

## *4.2. Initial rotational stiffness*

### *4.2.1. Model assumptions*

The flange is subjected to the following set of distributed loads (line loads) as depicted in Figure 25-a:

- The contact forces $f_c$ exerted on the lower face of the flange in the compression area,
- A distributed force $b$ exerted by the bolts on the upper face of the flange in the tensile zone,
- The prying force $q$ exerted on the lower face of the flange in the tensile area.

The above loading is statically equivalent to a concentrated normal force $N$ placed at the centroid of the tube and a bending moment $M_j$ at the same location. The tensile force $f_T$ applied by the tube-wall to the flange is in longitudinal equilibrium with the bolt and the prying forces. Moreover, the tube-wall exert a compressive force, $f_C$, on the flange in the compression area. In presence of thick flanges, the prying force may not exist and only the bolts load the flange in the tensile area. The bolt forces are then equal to the tensile forces applied by the tube-wall to the flange and create a local bending moment at the junction between the tube-wall and the flange. This assumption has been considered by Stamatopoulos [12] and Kozlowski et al [13] either for the evaluation of the bending resistance or the initial rotational stiffness. In presence of thin flange, the prying force always exist and tend to decrease the bending moment at the junction with the tube-wall created by the bolt forces. In order to avoid complex calculations involving bolt and prying forces, the tensile force is applied at a radius $R_{t,el}$ such as it reproduces the same local bending moment at the junction between the tube-wall and the flange (see Figure 25-b).

This radius will be defined in section 4.2.5. In the meantime, the contact stress distribution is replaced by a line force $f_c$ located at a radius $R_c$ that will be determined in section 4.2.4.

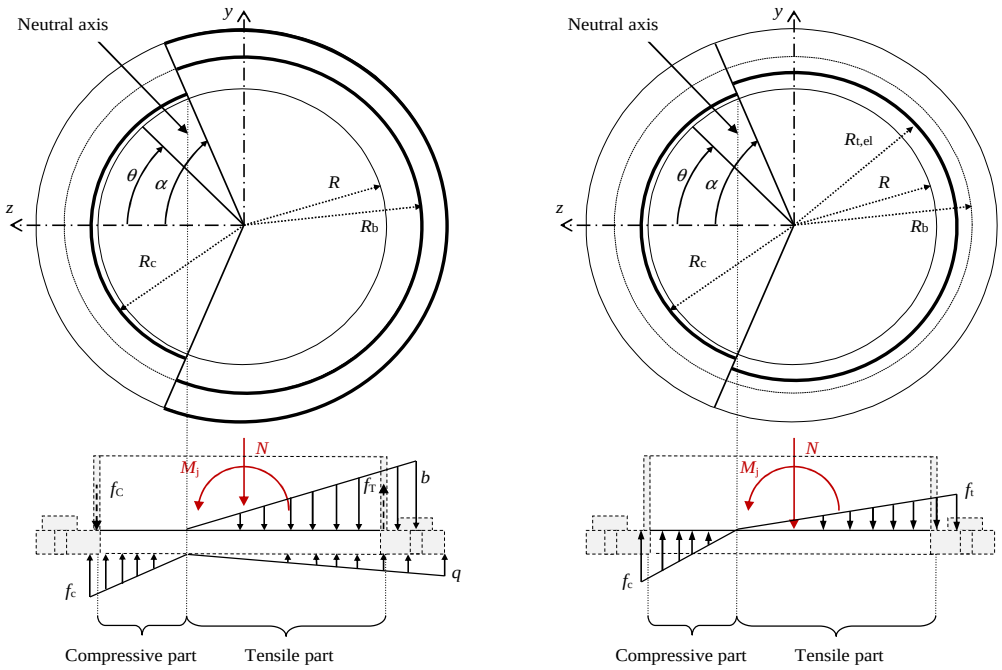


*a- Contact force applied to the flange* *b- Equivalent forces applied to the flange*

***Figure 25.*** *Forces applied to the connection*

The cross-section at the junction between the tube wall and the flange (see Figure 26) is supposed to be rigid in its own plane and to remain plane during loading (Bernoulli assumption). A rotation $\phi_j$ is applied to this cross-section and the interaction between the flange and the tube wall is modelled considering springs placed along the circumference of the tube. The springs have different stiffness in tension and in compression. The distribution of the forces applied by the tube wall to the flange is then linear in both compression and tension zones.

Considering the plane cross-section assumption, the displacement of the flange at the junction with the tube-wall (see Figure 26) can be expressed as follows:

$$\delta(\theta) = \begin{cases} -\delta_{c,m} \dfrac{\cos\theta - \cos\alpha}{1 - \cos\alpha} & \text{for} \quad 0 \le \theta \le \alpha \\ \delta_{t,m} \dfrac{\cos\alpha - \cos\theta}{\cos\alpha + 1} & \text{for} \quad \alpha \le \theta \le \pi \end{cases} \tag{3}$$

where $\delta_{c,m}$ is the maximum displacement in the compressive zone ($\theta = 0$), $\alpha$ the angle defining the position of the neutral axis and $\delta_{t,m}$ the maximum displacement in the tensile zone ($\theta = \pi$).

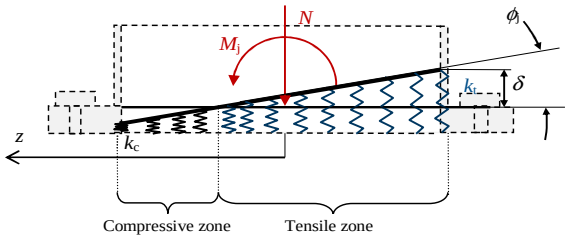


***Figure 26.*** *Deformation of the connection with a dominant bending moment*

The displacement $\delta_{t,m}$ and $\delta_{c,m}$ can be expressed as function of the rotation $\phi_j$ of the connection:

$$\delta_{t,m} = R\ (1+\cos\alpha)\phi_j \tag{4}$$

$$\delta_{c,m} = R(1-\cos\alpha)\phi_j \tag{5}$$

The relation between the distributed force applied by the tube-wall and the displacement is:

$$f_t(\theta) = k\delta(\theta) \tag{6}$$

where $k$ is a stiffness coefficient per unit length; equal to $k_t$ in the tensile zone and to $k_c$ in the compressive zone, respectively.

These stiffness coefficients are calculated via L-stub models presented in sections 4.2.4 and 4.2.5 for the compressive and tensile parts, respectively.

Let $f_{T,m}$ be the maximal force per unit length applied by the tube-wall in the tensile area ($\theta = \pi$) and $f_{C,m}$ the maximal force per unit length applied by the tube-wall in the compressive area ($\theta = 0$). These forces are related to the maximum displacements $\delta_{t,m}$ and $\delta_{c,m}$ through

$$f_{T,m} = k_t\delta_{t,m} \tag{7}$$

$$f_{C,m} = k_c\delta_{c,m} \tag{8}$$

Due to circumferential symmetry, the relation between the force applied by the tube-wall and those on the flange are:

$$f_{t,m} = f_{T,m}\frac{R}{R_{t,el}} \tag{9}$$

$$f_{c,m} = f_{C,m}\frac{R}{R_c} \tag{10}$$

where $f_{t,m}$ is the maximal force applied on the flange in the tensile area ($\theta = \pi$) and $f_{c,m}$ the maximal force applied to the flange in the compressive area ($\theta = 0$).

The ratio between $f_{t,m}$ and $f_{c,m}$ reads:

$$\frac{f_{t,m}}{f_{c,m}} = \frac{k_t}{k_c}\frac{R_c}{R_{t,el}}\frac{1+\cos\alpha}{1-\cos\alpha} = m_k\frac{R_c}{R_{t,el}}\frac{1+\cos\alpha}{1-\cos\alpha} \tag{11}$$

The force applied to the flange can be expressed as:

$$f(\theta) = \begin{cases} f_{c,m}\dfrac{\cos\theta-\cos\alpha}{1-\cos\alpha} & \text{for} \quad 0 \le \theta \le \alpha \\ f_{t,m}\dfrac{\cos\alpha-\cos\theta}{\cos\alpha+1} & \text{for} \quad \alpha \le \theta \le \pi \end{cases} \tag{12}$$

Finally, regarding the connection behaviour, two cases are possible:

- The bending moment is dominant and both a compressive and a tensile zone develop. It is therefore necessary to find the position of the neutral axis, which depends on the loading and the relative stiffness of the tensile and compressive parts of the connection,
- The axial force is dominant and large enough to produce tension or compression over the whole cross-section.

The initial rotational stiffness $S_{j,ini}$ is defined as the ratio between the bending moment $M_j$ and the connection rotation $\phi_j$:

$$S_{j,ini} = \frac{M_j}{\phi_j} \tag{13}$$

### *4.2.2. Position of the neutral axis*

If the bending moment is dominant, the stress distribution comprises a compressive and a tensile zone as indicated in Figure 26. Considering Eq (12), the axial forces generated by the compressive and the tensile stresses are given by:

$$F_{t,tot} = 2\int_{\alpha}^{\pi} f(\theta)R_{t,el}\,d\theta = 2R_{t,el}f_{t,m}\frac{\sin\alpha+(\pi-\alpha)\cos\alpha}{1+\cos\alpha} \tag{14}$$

$$F_{c,tot} = 2\int_0^{\alpha} f(\theta) R_c d\theta = 2R_c f_{c,m} \frac{\sin\alpha - \alpha\cos\alpha}{1-\cos\alpha} \tag{15}$$

The equilibrium in the longitudinal direction gives:

$$N = F_{c,tot} - F_{t,tot} \tag{16}$$

Inserting equations Eqs (11), (14) and (15) in (16), we get the expression of $f_{c,m}$ as a function of $N$ and $\alpha$:

$$f_{c,m} = \frac{N}{2R_c} \frac{1-\cos\alpha}{\sin\alpha - \alpha\cos\alpha - m_k\left(\sin\alpha + (\pi-\alpha)\cos\alpha\right)} \tag{17}$$

The bending moments about the neutral axis produced by the compressive and tensile forces, respectively, are given by:

$$M_{j,c} = 2\int_0^{\alpha} f(\theta) d_c(\theta) R_c d\theta = R_c^{\,2} f_{c,m} \frac{\alpha - \cos\alpha\sin\alpha}{1-\cos\alpha} - F_{c,tot} R_c \cos\alpha \tag{18}$$

$$M_{j,t} = 2\int_{\alpha}^{\pi} f(\theta) d_t(\theta) R_{t,el} d\theta = R_{t,el}^2 f_{t,m} \frac{\pi - \alpha + \cos\alpha\sin\alpha}{1+\cos\alpha} + F_{t,tot} R_c \cos\alpha \tag{19}$$

where $d_c$ and $d_t$ are the distances between the neutral axis and the line forces:

$$d_c(\theta) = R_c\left(\cos\theta - \cos\alpha\right)$$
$$d_t(\theta) = R_c\cos\alpha - R_{t,el}\cos\theta$$

The total bending moment $M_j$ reads:

$$M_j = M_{j,t} + M_{j,c} + NR_c\cos\alpha \tag{20}$$

Finally, the bending moment has the following expression:

$$M_j = R_c^2 f_{c,m} \frac{\alpha - \cos\alpha\sin\alpha}{1-\cos\alpha} + R_{t,el}^2 f_{t,m} \frac{\pi - \alpha + \cos\alpha\sin\alpha}{1+\cos\alpha} \tag{21}$$

Inserting expression of $f_{c,m}$ in (21), one obtains an equation for $\alpha$:

$$e_N = \frac{R_c(\alpha - \cos\alpha\sin\alpha) + m_k R_{t,el}\left(\pi - \alpha + \cos\alpha\sin\alpha\right)}{2\left(\sin\alpha - \alpha\cos\alpha - m_k\left(\sin\alpha + (\pi-\alpha)\cos\alpha\right)\right)} \tag{22}$$

where $e_N$ is the eccentricity :

$$e_N = \frac{M_j}{N}$$

The angle $\alpha$ being comprised between 0 and $\pi$, the corresponding eccentricity is greater than $R_c/2$ or less than $-R_{t,el}/2$. For other values of the eccentricity, the flange is completely in tension ($-R_{t,el}/2 \le e_N \le 0$) or completely in compression ($0 \le e_N \le R_c/2$).

### *4.2.3. Initial rotational stiffness*

- **Dominant bending moment**

When the bending moment is dominant, Eq (4) to Eq (10) can be combined together to yield:

$$f_{t,m} = k_t \; R \; (1+\cos\alpha)\phi_j \frac{R}{R_{t,el}} \tag{23}$$

$$f_{c,m} = k_c \; R \; (1-\cos\alpha)\phi_j \frac{R}{R_c} \tag{24}$$

Inserting (23) and (24) into (21), the expression of the bending moment applied by the tube to the connection becomes:

$$M_j = \phi_j R^2 \left[ R_c k_c \left( \alpha - \frac{\sin 2\alpha}{2} \right) + R_{t,el} k_t \left( \pi - \alpha + \frac{\sin 2\alpha}{2} \right) \right] \tag{25}$$

Thus the initial rotational stiffness of the connection is:

$$S_{j,ini} = R^2 \left[ R_c k_c \left( \alpha - \frac{\sin 2\alpha}{2} \right) + R_{t,el} k_t \left( \pi - \alpha + \frac{\sin 2\alpha}{2} \right) \right] \tag{26}$$

The above expression is a function solely of $\alpha$ which can be obtained solving equation (22) and is comprised between 0 and $\pi$. Outside this range, the axial force is dominant and the connection is completely in tension or completely in compression.

- **Dominant axial force**

When the axial force is dominant, the stiffness is the same along the circumference of the connection and is equal to either $k_t$ or $k_c$. The rotation is directly related to the displacement of the flange produced by the bending moment. Considering the plane cross-section assumption, the displacement $\delta$ is given by (see Figure 27):

$$\delta(\theta) = -\phi_j R \cos\theta \tag{27}$$

The initial rotational stiffness is:

for a dominant compressive force ($0 \le e_N \le R_c/2$):

$$S_{j,c} = k_c R^2 R_c \pi \tag{28}$$

for a dominant tensile force ( $-R_{t,el}/2 \le e_N \le 0$ ):

$$S_{j,t} = k_t R^2 R_{t,el} \pi \tag{29}$$

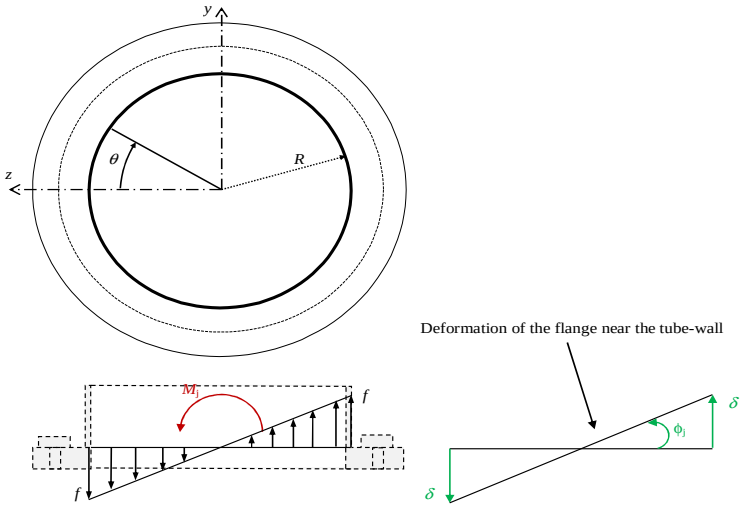


***Figure 27.*** *Deformation of the connection due to bending with a dominant axial force*

*4.2.4. Stiffness of the compressive part*

The stiffness of the compressive component corresponds to the ratio between the force applied by the tube wall to the flange $f_C$ and the displacement of the flange $\delta_c$. Kozlowski & Wojnar [13] proposed a formulation based on a parametric study for three types of welds. A theoretical solution is proposed here for full penetration butt welds of ring and blank flanges (see Figure 28).

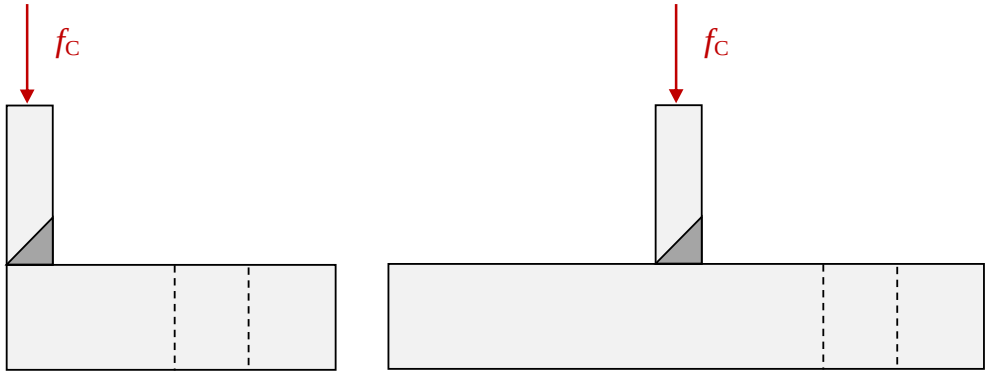


*a- L-stub : ring flange* *b- T-stub : blank flange*

***Figure 28.*** *L-stubs and T-stubs in compression*

- *Full penetration butt welds of ring flanges : L-stub in compression*

The opposite flanges in contact are modelled via the model proposed by Couchaux et al ([24], [25]) for beams in frictionless contact with a rigid foundation. The latter corresponds to the transverse plane of symmetry passing through the opposite flanges. Stamatopoulos & Ermopoulos [11] investigated a flange subjected to a compressive force when the yield strength is reached at the tube-wall and proposed, based on numerical simulations, the following expression for the contact pressure:

$$\begin{aligned} p(x) &= p_{\max} && \text{for} \quad -t_t/2 \le x \le t_t/2 \\ p(x) &= p_{\max}\frac{\xi_c + t_t/2 - x}{\xi_c} && \text{for} \quad t_t/2 \le x \le \xi_c + t_t/2 \end{aligned} \tag{30}$$

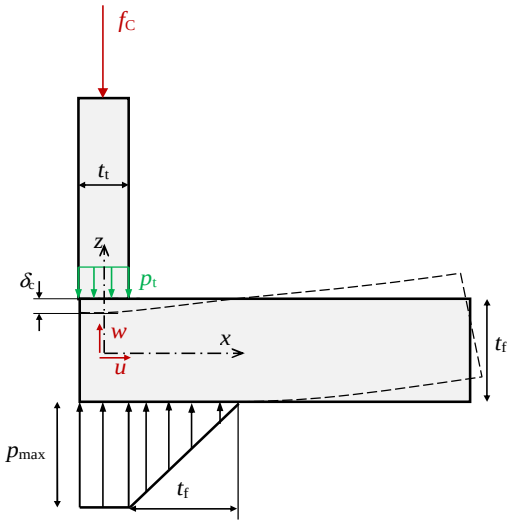


***Figure 29.*** *L-stub in compression*

These expressions of the contact pressure will be adopted to simplify the analytical expressions and $\xi_c \approx 0{,}98 t_f$ will be considered equal to $t_f$. Hence, if the flange in contact with a rigid support is modelled via the mechanical model proposed by Couchaux et al [25], the deflection $w$ at the tube-wall junction is:

$$w(x,z) = \frac{1}{4}\left[2z - 3\frac{z^2}{t_f} + 2\frac{z^4}{t_f^3}\right]\frac{(p_t - p_{\max})}{E} - \frac{p_t z}{E} - \frac{6\nu z^2}{E t_f^3} M(x) + w_1(x) \tag{31}$$

where $M(x)$ is the bending moment per unit length in the flange, $w_1(x)$ the deflection at $z = 0$. Its expression is given by:

$$w_1(x) = -\frac{t_f}{32E}\left[13p_{max} + 3p_t\right] + \frac{3\nu}{2Et_f}M(x) \tag{32}$$

Hence the transverse displacement of the flange at the junction with the tube-wall is:

$$\delta_c = -w(0,\ t_f/2) = t_f\,\frac{p_{max} + p_t}{2E} \tag{33}$$

Considering equilibrium in the longitudinal direction, one obtains:

$$p_{max} = \frac{f_C}{t_t + \frac{t_f}{2}} \tag{34}$$

$$p_t = \frac{f_C}{t_t} \tag{35}$$

Inserting (34) and (35) into (33), we get the stiffness per unit length of an L-stub in compression:

$$k_c = \frac{f_C}{\delta_c} = -\frac{f_C}{w(0,\ t_f/2)} = E\,\frac{\lambda_t(2\lambda_t + 1)}{2\lambda_t + 1/2} \tag{36}$$

with $\lambda_t = \frac{t_t}{t_f}$.

The distance between the resultant of the contact stresses and the centre of the tube is:

$$R_c = R + \frac{t_f}{2}\,\frac{\lambda_t + 2/3}{2\lambda_t + 1} \tag{37}$$

- *Full penetration butt welds of blank flanges : T-stub in compression*

The component in compression of a blank flange is modelled via a T-stub in contact with a rigid support and subjected to a compressive force (see Figure 30). The maximum contact pressure is thus:

$$p_{max} = \frac{f_C}{t_t + t_f} \tag{38}$$

Finally, the stiffness per unit length of a T-stub in compression is:

$$k_c = E\,\frac{2\lambda_t(\lambda_t + 1)}{2\lambda_t + 1} \tag{39}$$

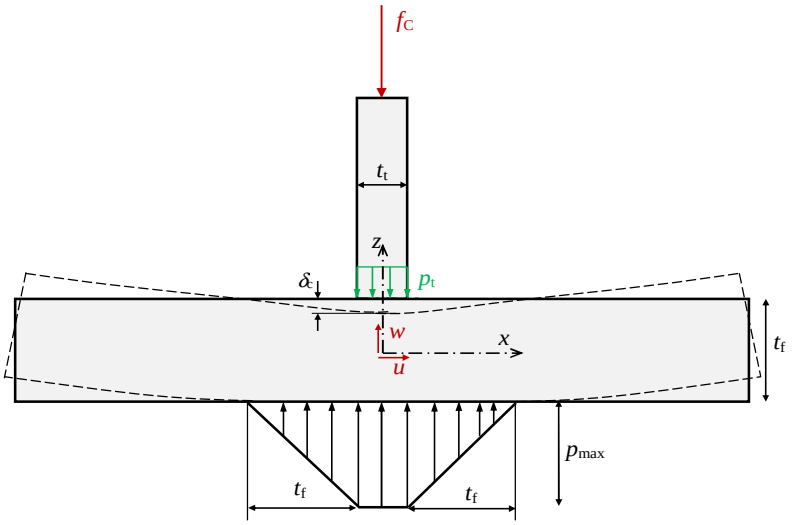


***Figure 30.*** *T-stub in compression*

*4.2.5. Stiffness of the tensile part*

The stiffness of the component in tension corresponds to the ratio between the tensile force applied by the tube wall to the flange $f_T$ and the displacement of the flange $\delta_t$.

The evaluation of the stiffness is based on the model proposed for L-stubs by Couchaux et al [24] and presented in Figure 31. The flange rotation is prevented by the tube-wall, and the effect of the bolt is modelled by an axial spring. The stiffness of the bolt is defined according to EN 1993-1-8 rules:

$$k_b = \frac{EA_s}{L_b / 2} \tag{40}$$

where $L_b$ is the tensile bolt length calculated via EN 1993-1-8 [26] and $A_s$ its cross-section area.

The flange is in pointwise contact at a point located between the bolt axis and the outer edge of the flange which corresponds to the point of application of the prying force. The prying force is also positioned at a distance $n$ from the bolt axis as suggested by Couchaux et al [24]:

$$n = \min\left[\left(2e_2 + \xi\right)/3;\ \xi + 0{,}74t_f\right] \tag{41}$$

with

$$\xi = e_2\sqrt{\frac{\alpha_{R,0}}{\alpha_R}} \le e_2$$

$$\alpha_{\mathrm{R}} = 4\left(\frac{e_1}{t_{\mathrm{f}}}\right)^3 \frac{A_{\mathrm{s}}}{L_{\mathrm{b}} p_{\mathrm{b}}},\quad p_{\mathrm{b}} = \frac{2\pi R}{n_{\mathrm{b}}},\quad \alpha_{\mathrm{R},0} = \frac{e_2/e_1 + 1}{(e_2/e_1)^3}.$$

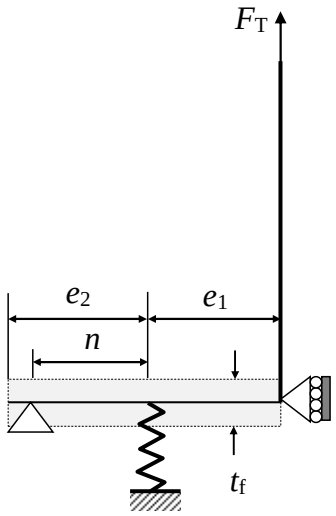


***Figure 31 :*** *Model for L-stubs in tension*

To simplify the analysis, the response of the flange is studied considering the mechanical model presented in Figure 32 where the vertical support at the free edge corresponding to a point-wise contact has been moved to the junction between the flange and the tube and supplemented by a torsional spring that reproduces the flexural interaction between the tube-wall and the flange. The expression of the stiffness of the rotational spring is:

$$k_\theta = 2\beta D_{\mathrm{t}} p_{\mathrm{b}} \tag{42}$$

with

$$\beta = \sqrt[4]{\frac{3(1-\nu^2)}{R^2 t_{\mathrm{t}}^2}},\ D_{\mathrm{t}} = \frac{E t_{\mathrm{t}}^3}{12(1-\nu^2)}.$$

In presence of blank flange, the elastic restrain due to the portion of flange present inside the tube can be considered via the circular plate bending theory:

$$k_\theta = \left(2\beta D_{\mathrm{t}} + D_{\mathrm{f}}(1+\nu)/R\right) p_{\mathrm{b}} \tag{43}$$

with

$$D_{\mathrm{f}} = \frac{E t_{\mathrm{f}}^3}{12(1-\nu^2)}.$$

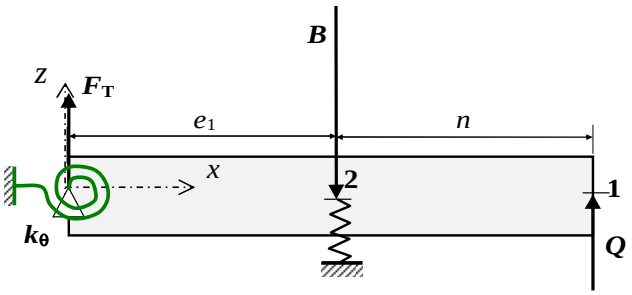


***Figure 32 :*** *Analysis of the L-stub*

The flange is subjected to the bolt force $B$ and the prying force $Q$. These forces are in equilibrium with the applied tensile force $F_T$. In the meantime, compatibility between the bolt and the flange has to be fulfilled. The prying force and the bolt force act at point 1 and point 2, respectively. Under a unit prying force ($Q$ = 1) alone, the deflections at point 1 and at point 2 are taken to be $\delta_{Q1}$ and $\delta_{Q2,}$ respectively. Similarly, under a unit bolt force ($B$ = 1), the deflections at point 1 and at point 2 are taken to be $\delta_{B1}$ and $\delta_{B2}$, respectively. The total flange deflection at point 2 can be expressed as:

$$w_2 = Q\delta_{Q2} - B\delta_{B2} \tag{44}$$

with

$$\delta_{Q2} = \frac{e_1^2}{EI_f}\left(\frac{n}{2}+\frac{e_1}{3}\right)+e_1\left(\frac{1}{GA_f}+\frac{e_1+n}{k_\theta}\right),\ \delta_{B2} = \frac{e_1^3}{3EI_f}+e_1\left(\frac{1}{GA_f}+\frac{e_1}{k_\theta}\right),$$

$$I_f = \frac{p_b t_f^3}{12},\ A_f = 0{,}8\,p_b t_f$$

Similarly, the total flange deflection at point 1 is computed as:

$$w_1 = Q\delta_{Q1} - B\delta_{B1} \tag{45}$$

with $\delta_{Q1} = \dfrac{(e_1+n)^3}{3EI_f}+\dfrac{e_1+n}{GA_f}+\dfrac{(e_1+n)^2}{k_\theta}$ and $\delta_{B1} = \delta_{B2}+n\left(\dfrac{e_1^2}{2EI_f}+\dfrac{e_1}{k_\theta}\right)$.

Compatibility demands that the elongation of the bolt is equal to the difference between $w_1$ and $w_2$:

$$w_1 - w_2 = -\frac{B}{k_b} \tag{46}$$

Furthermore, equilibrium in the vertical direction gives:

$$B = F_T + Q \tag{47}$$

Combining equations (44) to (47), one obtains the relation between the bolt force and the tensile force:

$$B = \frac{\delta_{Q1} - \delta_{Q2}}{1/k_b + \delta_{Q1} - \delta_{Q2} - (\delta_{B1} - \delta_{B2})} F_T = \eta F_T \tag{48}$$

Finally, the stiffness of the tensile part is given by:

$$k_t = \frac{f_T}{\delta_t} = -\frac{F_T}{w_1 p_b} = \frac{1}{\left[\eta(\delta_{B1} - \delta_{Q1}) + \delta_{Q1}\right] p_b} \tag{49}$$

The bending moment at the junction between the tube-wall and the flange is equal to:

$$M_E = Be_1 - Q(e_1 + n) = F_T\left(\eta e_1 - (\eta - 1)(e_1 + n)\right) \tag{50}$$

The same bending moment can be obtained by applying the tensile force $F_T$ at a distance $x_{t,el}$ from the tube-wall :

$$x_{t,el} = \frac{M_E}{F_T} = \eta e_1 - (\eta - 1)(e_1 + n) \tag{51}$$

One obtain the equivalent radius of the tensile part considered in Figure 25-b:

$$R_{t,el} = x_{t,el} + R = \eta e_1 - (\eta - 1)(e_1 + n) + R \tag{52}$$

## *4.3. Plastic bending moment*

### *4.3.1. General hypothesis*

The failure mode depends on the ductility of the different components of the connection. We have chosen to consider two types of failure modes:

- A “ductile” failure mode (see Figure 33-a) where the full resistance of each component is reached,
- A “non-ductile” failure mode (see Figure 33-b) where the full resistance of the most stressed components of the connection is reached.

In section 4.3.2, we explain how to identify the relevant failure mode.

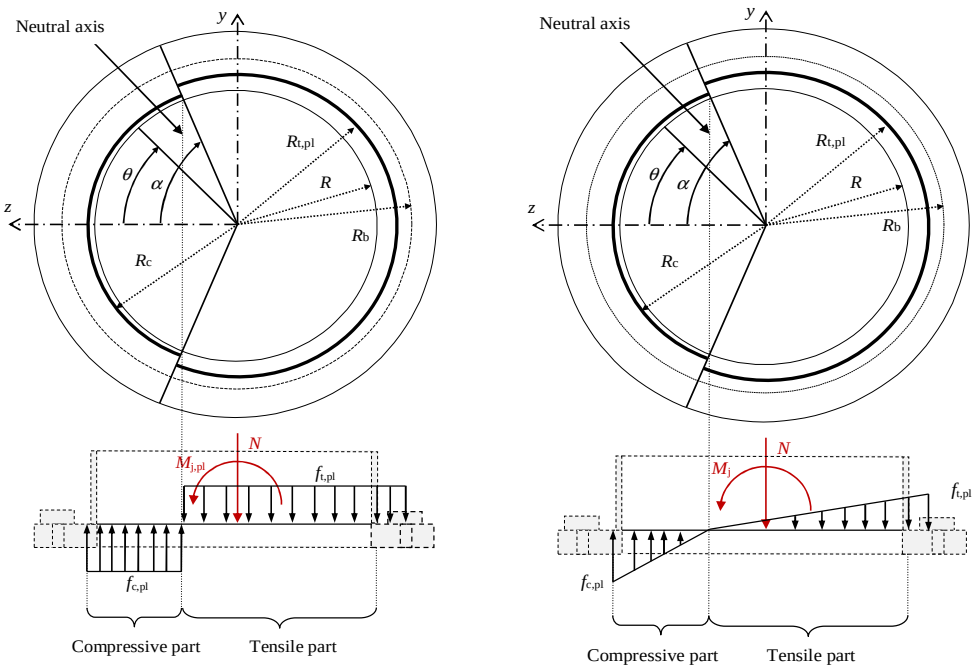


*a- "Ductile" failure mode* *b- "Non-ductile" failure mode*

***Figure 33 :*** *Distribution of forces for each failure modes*

A distributed force $f(\theta)$ is applied to the flange such as equilibrium with the bending moment and the axial force applied to the connection is fulfilled (see Figure 33 a and b). In a "ductile" failure mode, the resistance of each component of the connection is reached (see Figure 33-a), and thus we have the following expression for $f(\theta)$:

$$f(\theta) = \begin{cases} f_{c,pl}, & \text{for } 0 \le \theta \le \alpha \\ f_{t,pl}, & \text{for } \alpha \le \theta \le \pi \end{cases} \tag{53}$$

where

$f_{c,pl}$ is the compressive resistance per unit length (see section 4.3.6),

$f_{t,pl}$ is the tensile resistance per unit length (see section 4.3.5),

$\alpha$ is the angle defining the position of the neutral axis.

Such as for the evaluation of the rotational stiffness, the tensile forces are placed at a radius, $R_{t,pl}$, comprised between $R$ and $R_b$ to take into account the presence of prying force. The evaluation of $R_{t,pl}$ is explained in section 4.3.5 and depends on the failure mode of the tensile zone.

In a "non-ductile" failure mode, the resistances of the most stressed tensile and compressive components of the connection are reached (see Figure 33-b), which gives:

$$f(\theta) = \begin{cases} f_{c,pl} \dfrac{\cos\theta - \cos\alpha}{1 - \cos\alpha}, & \text{for } 0 \le \theta \le \alpha \\ f_{t,pl} \dfrac{\cos\alpha - \cos\theta}{\cos\alpha + 1}, & \text{for } \alpha \le \theta \le \pi \end{cases} \tag{54}$$

For these two failure modes, the position of the neutral axis, defined by the angle α, will be determined considering the axial equilibrium equation:

$$N = F_{c,pl,tot} - F_{t,pl,tot} \tag{55}$$

where

$F_{c,pl,tot}$ is the resultant of the compressive part, $F_{t,pl,tot}$ the resultant of the tensile part and $N$ the axial force.

Furthermore, the bending moment acting on the connection is:

$$M_{j,pl} = M_{j,t,pl} + M_{j,c,pl} + NR_c \cos\alpha \tag{56}$$

where $M_{j,c,pl}$ is the resultant bending moment arising from the compressive part evaluated at the neutral axis,

$M_{j,t,pl}$ is the resultant bending moment arising from the tensile part evaluated at the neutral axis

### *4.3.2. Ductility of the connection*

Each connection components will reach its resistance only if the most deformed components are sufficiently ductile in both tensile and compressive parts. It is obvious that the tensile part of the connection is not ductile when its failure mode corresponds to the rupture of bolts without prying action. On the other hand, the compressive part of the connection is ductile when the tube is class 1 or 2. However, even if the class of the tube is 3 or 4, the tensile part of the connection, when sufficiently ductile, can reach its entire potential resistance if its resistance is significantly lower than that of the compressive part of the connection. Finally, with the benefit of a series of comparisons with numerical and experimental results, the authors have chosen that a connection can be classified as "non-ductile" if one of the following condition is fulfilled:

- The class of the tube is 4 according to proposal of Rotter & Sadowski [27] and prEN 1993-1-1 [29] (see Eq. (57)) and the ultimate tensile resistance of the connection increased of 20% is greater than the compressive resistance of the tube $N_{c,pl}$,
- The ultimate tensile resistance of the connection is greater than 95% of the sum of the tensile resistance of the bolts.

The boundary between class 3 and 4 is:

$$\left.\frac{D}{t_t}\right|_{lim} = a_3 = a_{3,0} k_N \tag{57}$$

where $a_{3,0}$ is the boundary proposed by Rotter & Sadowski [27] for pure bending:

$$a_{3,0} = \min\left( \max\left( 83\left[ 2,48 - \frac{L_1}{D}\sqrt{\frac{t_t}{D}} \right];\ 140 \right);\ 190 \right)\varepsilon^2$$

$$\varepsilon = \sqrt{\frac{235}{f_{y,t}}}$$

$k_N$ is a reduction factor that consider axial force based on prEN 1993-1-1[29] :

$$k_N = \frac{18}{5\psi + 23}$$

$\psi$ is the ratio between minimal and maximal stresses on the tube.

### *4.3.3. Ductile failure mode*

When the failure mode is “ductile”, the resultant of the compressive and tensile forces are obtained from (53):

$$F_{c,pl,tot} = 2\int_0^{\alpha} f_{c,pl} R_c d\theta = 2\alpha R_c\ f_{c,pl} \tag{58}$$

$$F_{t,pl,tot} = 2\int_{\alpha}^{\pi} f_{t,pl} R_{t,pl} d\theta = 2(\pi - \alpha) R_{t,pl}\ f_{t,pl} \tag{59}$$

Inserting the resultant forces (58) and (59) into the axial equilibrium equation (55) and considering Eqs (71) and (76) one obtain an expression for the angle $\alpha$ defining the position of the neutral axis:

$$\frac{\alpha}{\pi} = \frac{N + N_{T,pl}}{N_{c,pl} + N_{T,pl}} \tag{60}$$

One observes that the position of the neutral axis depends on the axial force, the compressive and tensile resistances of the connection. When the connection is entirely in tension ($N$=-$N_{T,pl}$), $\alpha$ is equal to 0. On the other hand, when the connection is entirely in compression ($N$=$N_{c,pl}$), $\alpha$ is equal to π. Similarly to the axial load $N$, the bending moments produced by the compressive and tensile parts of the connection $M_{j,c,pl}$ and $M_{j,t,pl}$ are:

$$M_{j,c,pl} = 2\int_0^{\alpha} f(\theta) d_c(\theta) R_c d\theta = N_{c,pl} R_c \frac{\sin\alpha - \alpha\cos\alpha}{\pi} \tag{61}$$

$$M_{j,t,pl} = 2\int_{\alpha}^{\pi} f(\theta) d_t(\theta) R_{t,pl} d\theta = N_{T,pl} \frac{\sin\alpha R_{t,pl} + (\pi - \alpha)\cos\alpha R_c}{\pi} \tag{62}$$

where $d_c$ and $d_t$ are the distances between the neutral axis and the forces per unit length:

$$d_c(\theta) = R_c\left(\cos\theta - \cos\alpha\right)$$
$$d_t(\theta) = R_c\cos\alpha - R_{t,pl}\cos\theta$$

Inserting Eq (61) and Eq (62) into Eq (56), we get the plastic bending moment:

$$M_{j,pl} = M_{j,pl,D}\sin\alpha \tag{63}$$

with $M_{j,pl,D} = \frac{N_{T,pl}R_{t,pl} + N_{c,pl}R_c}{\pi}$.

The plastic bending moment is related to $M_{j,pl,D}$ and to the angle $\alpha$ which itself depends on the axial force $N$.

### *4.3.4. Non ductile failure mode*

#### *4.3.4.1. Dominant bending moment*

When the failure mode is “non-ductile” and the bending moment is dominant, the resultant forces in the compressive and the tensile parts have the following expressions:

$$F_{c,pl,tot} = 2\int_0^{\alpha} f(\theta) R_c d\theta = \frac{N_{c,pl}}{\pi}\frac{\sin\alpha - \alpha\cos\alpha}{1 - \cos\alpha} \tag{64}$$

$$F_{t,pl,tot} = 2\int_{\alpha}^{\pi} f(\theta) R_{t,pl} d\theta = \frac{N_{T,pl}}{\pi}\frac{\sin\alpha + (\pi - \alpha)\cos\alpha}{1 + \cos\alpha} \tag{65}$$

Inserting Eqs (64) and (65) into the axial equilibrium equation (55), we get an equation where the angle $\alpha$ is the unknown variable

$$\frac{N}{N_{\mathrm{T,pl}}} = \frac{N_{\mathrm{c,pl}}}{N_{\mathrm{T,pl}}}\frac{1}{\pi}\frac{\sin\alpha - \alpha\cos\alpha}{1-\cos\alpha} - \frac{1}{\pi}\frac{\sin\alpha + (\pi-\alpha)\cos\alpha}{1+\cos\alpha} \tag{66}$$

An explicit expression for the angle $\alpha$ cannot be determined from this equation and only a numerical solution can be obtained. The bending moments resulting from the compressive and tensile parts of the connection $M_{\mathrm{j,c,pl}}$ and $M_{\mathrm{j,t,pl}}$ are:

$$M_{\mathrm{j,c,pl}} = 2\int_0^{\alpha} f(\theta) d_{\mathrm{c}}(\theta) R_{\mathrm{c}} d\theta = \frac{N_{\mathrm{c,pl}} R_{\mathrm{c}}}{2\pi}\frac{\alpha - \cos\alpha\sin\alpha}{1-\cos\alpha} - F_{\mathrm{c,pl,tot}} R_{\mathrm{c}}\cos\alpha \tag{67}$$

$$M_{\mathrm{j,t,pl}} = 2\int_{\alpha}^{\pi} f(\theta) d_{\mathrm{t}}(\theta) R_{\mathrm{t,pl}} d\theta = \frac{N_{\mathrm{T,pl}} R_{\mathrm{t,pl}}}{2\pi}\frac{\pi - \alpha + \cos\alpha\sin\alpha}{1+\cos\alpha} + F_{\mathrm{t,pl,tot}} R_{\mathrm{c}}\cos\alpha \tag{68}$$

Inserting Eq (67) and Eq (68) into Eq (56), we get the closed form expression for the plastic bending moment:

$$M_{\mathrm{j,pl}} = \frac{N_{\mathrm{c,pl}} R_{\mathrm{c}}}{2\pi}\frac{\alpha - \cos\alpha\sin\alpha}{1-\cos\alpha} + \frac{N_{\mathrm{T,pl}} R_{\mathrm{t,pl}}}{2\pi}\frac{\pi - \alpha + \cos\alpha\sin\alpha}{1+\cos\alpha} \tag{69}$$

The latter expression can be used for all the values of $N$ comprised between $N_{\mathrm{c,pl}}/2$ and $-N_{\mathrm{T,pl}}/2$. When that condition is not fulfilled, the axial force is dominant and the connection is either completely in tension or in compression.

*4.3.4.2. Dominant axial force (tension/compression)*

When the axial force is dominant, the ultimate state is reached in the most stressed part of the connection, and the plastic bending moment becomes:

$$M_{\mathrm{j,pl}} = \begin{cases} \dfrac{N_{\mathrm{c,pl}} R_{\mathrm{c}}}{2}\left[1 - \dfrac{N}{N_{\mathrm{c,pl}}}\right] & \text{for} \quad N_{\mathrm{c,pl}}/2 \le N \le N_{\mathrm{c,pl}} \\ \dfrac{N_{\mathrm{T,pl}} R_{\mathrm{t,pl}}}{2}\left[1 + \dfrac{N}{N_{\mathrm{T,pl}}}\right] & \text{for} \quad -N_{\mathrm{T,pl}} \le N \le -N_{\mathrm{T,pl}}/2 \end{cases} \tag{70}$$

*4.3.5. Resistance of the tensile part*

The resistance per unit length of the tensile part of the connection, $f_{\mathrm{t,pl}}$, is derived from the pure tensile resistance of the connection:

$$f_{\mathrm{t,pl}} = \frac{N_{\mathrm{T,pl}}}{2\pi R_{\mathrm{t,pl}}} \tag{71}$$

where

$N_{T,pl}$ is the plastic resistance of the connection.

The tensile resistance of the connection can be determined via the L-stub model ([5], [6], [7]) or considering the circumferential symmetry of the circular flange [4]. In the present paper, the latter has been adopted. To evaluate the tensile resistance, four failure modes have been considered:

- **Mode 1:** plastic bending mechanism of the flange, the corresponding resistance is noted $N_{T,1,pl}$
- **Mode 2:** yielding of bolts with prying effect, the corresponding resistance is noted $N_{T,2,pl}$
- **Mode 3:** yielding of the bolts with full separation of the flange, the corresponding resistance is noted $N_{T,3,pl}$
- **Mode 4:** yielding of the tube in tension, the corresponding resistance is noted $N_{T,4,pl}$

The tensile resistance of the connection is the minimum between the four failure modes. As for the elastic analysis, the position of the tensile force that produces the same bending moment at the junction between the tube-wall and the flange is approximated by:

$$x_{t,pl} = \eta e_1 - (\eta - 1)(e_1 + n) \tag{72}$$

With

$$\eta = \frac{\sum B}{N_{T,pl}}$$

$\Sigma B$: Sum of bolt forces (see Figure 34),

One obtain the equivalent radius of the tensile part:

$$R_{t,pl} = x_{t,pl} + R = \eta e_1 - (\eta - 1)(e_1 + n) + R \tag{73}$$

The ratio $\eta$ depends on the failure mode of the connection. In presence of failure mode 3, the resistance is:

$$N_{T,3,pl} = \sum B_{pl} = \sum B \tag{74}$$

with $B_{pl}$ being the tensile resistance of one bolt.

Hence $x_{t,pl} = e_1$ and $R_{t,pl} = R_b$, the position of the tensile force coincides with the radius of the bolt pitch circle. This assumption has been considered by Stamatopoulos [12].

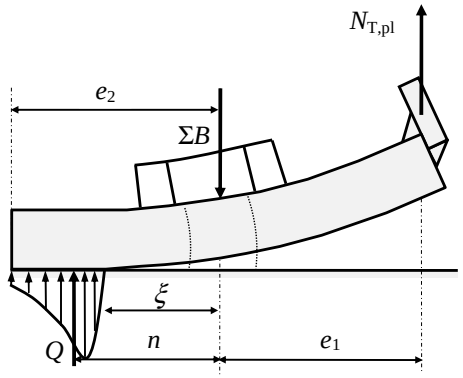


***Figure 34 :*** *Forces applied to the flanges*

In case failure mode 2 occurs, the sum of bolt forces is also equal to their tensile resistance, so the result is trivial. For failure mode 1, the sum of bolt forces is lower than their tensile resistance and the following expression has been proposed by Couchaux et al [4]:

$$\sum B = N_{T,1,pl} + 2\pi M_{pl,f} \frac{R_b}{R_e - R_b} \tag{75}$$

Where:

$R_e = R_b + n$

$M_{pl,f}$ : Plastic bending moment per unit length of the flange :

$$M_{pl,f} = \frac{t_f^2 f_{y,f}}{4}$$

For failure mode 4, the value obtained with an elastic analysis can be used.

### *4.3.6. Resistance of the compressive part*

Since the limit state is reached in the compressive part when the tube wall buckles or yields, the resistance per unit length of the compressive part of the connection $f_{c,pl}$ is derived from the compressive resistance of the tube:

$$f_{c,pl} = \frac{N_{c,pl}}{2\pi R_c} \tag{76}$$

where $N_{c,pl}$ is the compressive resistance of the tube evaluated according to Eurocode 3 [28] considering the classification for class 4 of Equation (57).

### *4.3.7. Comparison against numerical results*

In Table 7, the plastic bending resistance obtained via numerical analysis and the analytical model, noted $M_{j,pl,num}$ and $M_{j,pl,ana}$ respectively, are compared. In addition, the bending resistance of the tube calculated according to the equations of Rotter & Sadowski [27], noted $M_{t,Rk}$, has been added.

| Specimen | Numerical | | Analytical | | |
|---|---|---|---|---|---|
| | $N$ | $M_{j,pl,num}$ | $M_{j,pl,ana}$ | $M_{t,Rk}$ | $M_{j,pl,ana}/M_{j,pl,num}$ |
| | *kN* | *kNm* | *kNm* | *kNm* | - |
| M1 | 0 | 1469 | 1379 | 2396 | 0,94 |
| M2 | 0 | 1284 | 1179 | 2183 | 0,92 |
| M3 | 0 | 1158 | 1118 | 2396 | 0,97 |
| M4 | 0 | 905 | 782 | 2396 | 0,86 |
| M5 | 0 | 990 | 810 | 848 | 0,82 |
| M6 | 0 | 833 | 850 | 848 | 1,02 |
| M7 | 0 | 746 | 738 | 848 | 0,99 |
| M8 | 0 | 196 | 196 | 523 | 1,00 |
| M9 | 0 | 336 | 345 | 523 | 1,03 |
| M9-N=-0,5MN | -500 | 249 | 228 | 465 | 0,91 |
| M9-N=0,5MN | 500 | 405 | 401 | 379 | 0,99 |
| M9-N=1MN | 1000 | 424 | 412 | 302 | 0,97 |
| M10 | 0 | 523 | 581 | 523 | **1,11** |
| M10-N=-1MN | -1000 | 406 | 447 | 409 | 1,10 |
| M10-N=-2MN | -2000 | 226 | 192 | 275 | 0,85 |
| M10-N=1MN | 1000 | 406 | 351 | 302 | 0,87 |
| M10-N=2MN | 2000 | 281 | 150 | 148 | 0,53 |
| M11 | 0 | 568 | 667 | 523 | **1,17** |
| M12 | 0 | 2784 | 2994 | 3902 | 1,08 |
| M13 | 0 | 2732 | 2844 | 3902 | 1,04 |
| M14 | 0 | 2122 | 1864 | 3902 | 0,88 |
| M15 | 0 | 39 | 39 | 64 | 0,99 |
| M16 | 0 | 55 | 60 | 64 | 1,09 |
| M17 | 0 | 71 | 67 | 114 | 0,94 |
| M18 | 0 | 64 | 61 | 104 | 0,95 |
| M19 | 0 | 51 | 52 | 104 | 1,02 |
| M20 | 0 | 42 | 40 | 104 | 0,94 |

***Table 7 :*** *Plastic bending resistance: comparison to parametric study*

Good matching is obtained between the analytical model and the numerical results with a mean value of the ratio $M_{j,pl,ana}/M_{j,pl,num}$ equal to 0,96. The analytical model seems slightly

unsafe for some specimens (M10 and M11), however the bending resistance obtained with the numerical simulations is close to the bending moment resistance of the tube with a failure mode corresponding to buckling of the tube-wall. In presence of axial force, the bending resistance of the tube calculated according to Rotter & Sadowski [27] is clearly below that obtained numerically.

### *4.4. Ultimate bending moment*

The ultimate bending resistance, $M_{j,u}$, is evaluated with the model developed in section 4.3. However, the plastic resistance in tension $N_{T,pl}$ is replaced with the ultimate resistance in tension $N_{T,u}$ as proposed by Couchaux et al [4]. However the engineering ultimate tensile stress is used instead of the true ultimate tensile stress for the evaluation of failure modes 1 and 2 as the tube-wall buckles before developing such high stresses. In Table 8, the ultimate bending resistances obtained via numerical analysis and the analytical model, noted $M_{j,u,num}$ and $M_{j,u,ana}$ respectively, are compared. The bending resistance of the tube is also given.

| Specimen | Numerical | | | Analytical | | |
|---|---|---|---|---|---|---|
| | $N$ | $M_{j,u,num}$ | $M_{j,u,ana}$ | $M_{t,Rk}$ | $M_{j,u,ana}/M_{j,u,num}$ | $M_{t,Rk}/M_{j,u,num}$ |
| | *kN* | *kNm* | *kNm* | *kNm* | - | - |
| M1 | 0 | 1809 | 1566 | 2396 | 0,87 | 1,32 |
| M2 | 0 | 1524 | 1357 | 2183 | 0,89 | 1,43 |
| M3 | 0 | 1529 | 1303 | 2396 | 0,85 | 1,57 |
| M4 | 0 | 1581 | 1049 | 2396 | 0,66 | 1,52 |
| M5 | 0 | 1079 | 875 | 848 | 0,81 | 0,79 |
| M6 | 0 | 943 | 968 | 848 | 1,03 | 0,90 |
| M7 | 0 | 882 | 862 | 848 | 0,98 | 0,96 |
| M8 | 0 | 313 | 264 | 523 | 0,84 | 1,67 |
| M9 | 0 | 413 | 447 | 523 | 1,08 | 1,27 |
| M9-N=-0,5MN | -500 | 424 | 354 | 465 | 0,83 | 1,10 |
| M9-N=0,5MN | 500 | 424 | 466 | 379 | 1,10 | 0,89 |
| M9-N=1MN | 1000 | 412 | 451 | 302 | 1,09 | 0,73 |
| M10 | 0 | 561 | 627 | 523 | 1,12 | **0,93** |
| M10-N=-1MN | -1000 | 541 | 523 | 409 | 0,97 | 0,76 |
| M10-N=-2MN | -2000 | 312 | 295 | 275 | 0,95 | 0,88 |
| M10-N=1MN | 1000 | 457 | 363 | 302 | 0,79 | 0,66 |
| M10-N=2MN | 2000 | 307 | 150 | 148 | 0,49 | 0,48 |
| M11 | 0 | 590 | 664 | 523 | 1,12 | **0,89** |
| M12 | 0 | 3402 | 3301 | 3902 | 0,97 | 1,15 |
| M13 | 0 | 3249 | 3129 | 3902 | 0,96 | 1,20 |
| M14 | 0 | 2917 | 2451 | 3902 | 0,84 | 1,34 |
| M15 | 0 | 49 | 46 | 64 | 0,94 | 1,30 |
| M16 | 0 | 60 | 69 | 64 | 1,14 | 1,06 |
| M17 | 0 | 85 | 81 | 114 | 0,95 | 1,33 |
| M18 | 0 | 78 | 73 | 104 | 0,94 | 1,34 |
| M19 | 0 | 64 | 63 | 104 | 0,99 | 1,63 |
| M20 | 0 | 54 | 48 | 104 | 0,89 | 1,94 |

***Table 8 :*** *Ultimate bending resistance: comparison to parametric study*

The mean value of the ratio $M_{j,u,ana}/M_{j,u,num}$ is equal to 0,93 The model is conservative for most investigated cases. The analytical model can be over conservative in presence of thin flanges (specimens M4 and M8 for example) due to the fact that the ultimate tensile resistance do not consider tying effect [4]. The model overestimate the ultimate resistance of specimens M10 and M11. However, the bending resistance of the tube seems closer to the numerical resistance.

In Table 9, the ultimate bending moment calculated according to the proposed model is compared against experimental results obtained by Yamaguchi [19], Jakubowski & Schmidt [20], Wang et al [21] and Pavlovic et al [22]. Again, the ultimate bending moment is underestimated for thin flanges (BL-L-TH12, BL-S-TH6 and 10). For some specimens tested by

Yamaguchi, the analytical model overestimated the ultimate resistance with failure caused by buckling of the tube-wall far from the connection [19]. In these particular cases, the bending resistance of the tube evaluated by the model of Rotter & Sadowski [27] provide accurate results.

| Reference | Specimen | Test | | Analytical | | | |
|---|---|---|---|---|---|---|---|
| | | $N$ | $M_{j,u,exp}$ | $M_{j,u,ana}$ | $M_{t,Rk}$ | $M_{j,u,ana}/M_{j,u,exp}$ | $M_{t,Rk}/M_{j,u,exp}$ |
| | | *kN* | *kNm* | *kNm* | *kNm* | - | - |
| - | INSA | 0 | 925 | 810 | 778 | 0,88 | 0,84 |
| Yamaguchi [19] | BL-L-TH12 | 0 | 134 | 121 | 158 | 0,90 | 1,18 |
| | BL-L-TH19 | 0 | 168 | 162 | 158 | 0,97 | 0,94 |
| | BL-L-TH22 | 0 | 166 | 163 | 158 | 0,98 | 0,95 |
| | BL-S-TH6 | 0 | 46 | 27 | 77 | 0,59 | 1,67 |
| | BL-S-TH10 | 0 | 68 | 60 | 77 | 0,89 | 1,13 |
| | BL-S-TH16 | 0 | 77 | 82 | 77 | 1,07 | 1,00 |
| | CL-S-TH10-P00 | 0 | 55 | 61 | 83 | 1,10 | 1,51 |
| | CL-S-TH22-P00 | 0 | 71,5 | 92 | 83 | 1,28 | 1,16 |
| | CL-S-TH22-P10 | -285 | 81 | 86 | 76 | 1,06 | 0,94 |
| | CL-S-TH22-P17 | -484 | 65 | 75 | 66 | 1,16 | 1,02 |
| Jakubowski [20] | VRF1 | 0 | 1870 | 1840 | 1662 | 0,98 | 0,89 |
| Wang et al [21] | J1 | 0 | 96 | 91 | 107 | 0,95 | 1,12 |
| Pavlovic et al [22] | FC1 | 0 | 2213 | 2142 | 1975 | 0,97 | 0,89 |

***Table 9 :*** *Ultimate bending resistance: comparison to experimental tests*

### *4.5. Moment-rotation curve*

The moment-rotation curve is fully characterized, as suggested in EN 1993-1-8, by the bending resistance and the initial rotational stiffness. The initial rotational stiffness is determined using expressions given in section 4.2. The plastic and ultimate bending moments are determined via the model presented in sections 4.3 and 4.4 respectively and consider two failure modes, ductile and non-ductile. The analytical expression of the moment-rotation curve is:

$$M_j = \begin{cases} S_{j,ini}\phi_j & \text{when} \quad 0 \le M_j \le M_{j,pl} \\ \left[ S_{j,ini}\phi_j {M_{j,pl}}^{\psi} \right]^{\frac{1}{\psi+1}} & \text{when} \quad M_{j,pl} \le M_j \le M_{j,u} \end{cases} \tag{77}$$

In EN 1993-1-8, $\psi$ is equal to 2,7 for bolted flange connections. The bolted circular flange connections can be classified in this category. However this formulation leads to an overestimation of the rotation capacity when the failure mode is non ductile (buckling just after the elastic range). Thus a value of $\psi$ equal to 1 is considered for non-ductile failure modes.

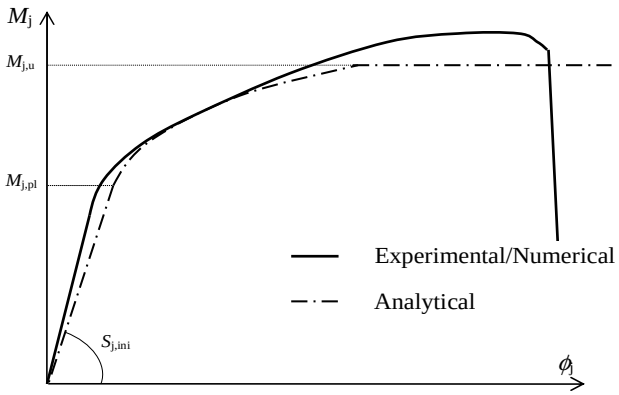


***Figure 35.*** *Analytical and experimental/numerical curves*

The moment-rotation curves calculated with the analytical model for connection M1, M8, M9 and M17 are compared against those obtained with numerical analyses in Figure 36.

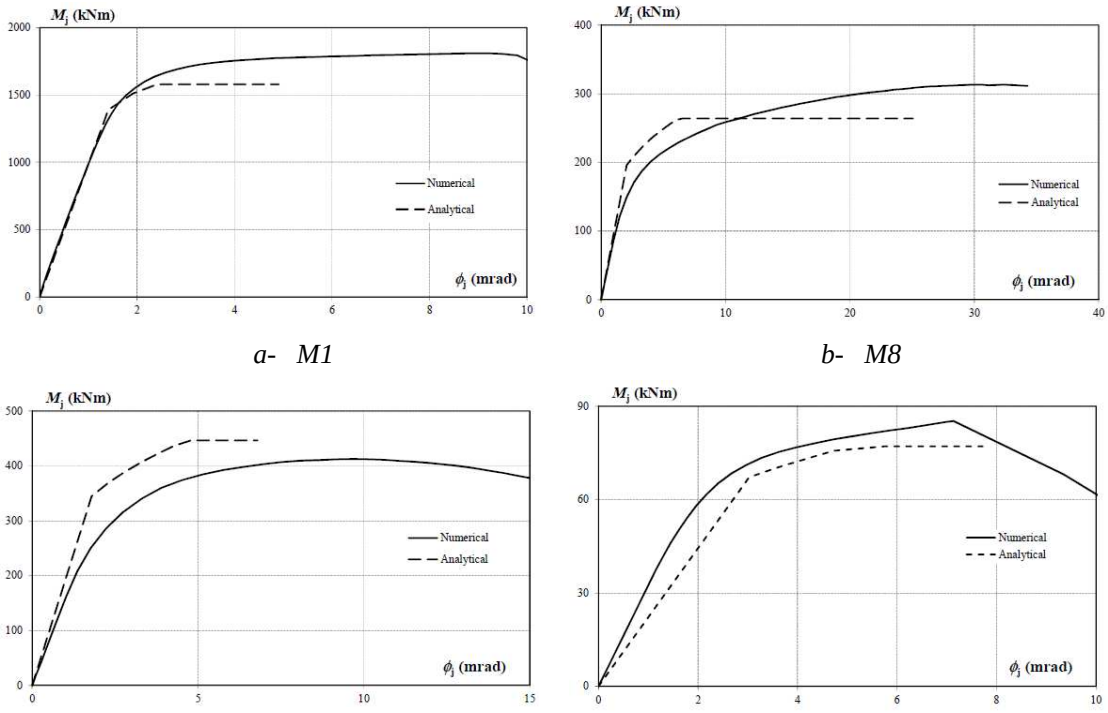


*a- M1* *b- M8*

*c- M9* *d- M17*

***Figure 36.*** *Moment-rotation curves*

The initial rotational stiffness is well estimated by the analytical model. For connection M17, the initial rotational stiffness is clearly underestimated. For this specimen, the diameter of the tube is smaller than for the other specimens (200 mm instead of 600-800 mm) and the circumferential symmetry neglected in the L-stub model plays an important. The model could

be improved considering the circular bending plate theory instead of the beam theory for the evaluation of the stiffness of the tensile part.

## *5. Conclusion*

An experimental test has been performed on one ring flange connection typically used in pylon of ski-lift. A non-ductile failure mode corresponding to local buckling of the tube-wall and yielding of three bolts in tension was observed. Initial imperfections of flanges seem to play an important role in the evolution of bolt forces during loading.

This experimental test has been completed by a set of finite element calculations using the code ANSYS. The FE model used solid and contact elements and permitted to observe plastic redistribution of bolt forces in presence of ductile failure modes. The influence of normal force and flange thickness on the bending resistances has also been investigated.

A closed-form expression for the moment-rotation curve has been proposed for bolted circular flange connections. This expression has been derived considering the initial rotational stiffness and the static bending resistance. A model, based on the component method, is proposed to determine the initial rotational stiffness and consider different stiffness in the tensile and compressive area. A new stiffness component, based on a beam model in contact with a rigid support, is evaluated for the compressive area and could be used for different connection configurations. The stiffness of the tensile zone is derived from L-stub model. The static resistance is determined for a combined bending moment and axial force (tension/compression). Two distributions of forces are considered to determine the plastic bending moment depending on the ductility of the tensile and the compressive parts of the connection. For the “ductile” failure mode, all the components reach their plastic resistance. For the “non-ductile” failure mode, only the most stressed components reach their resistance. The resistance calculated via this model compares well against those determined experimentally and numerically. It is worth to mention that the elastic model proposed in this paper is able to evaluate the force transferred by the most tensile bolt rows as well as the maximum tensile bolt force that can be used for a fatigue design. Particular attention should be given to the evaluation of the stress concentration factor at the weld toe between the tube wall and the flange. This requires further investigation.

## *6. References*

[1] Wardenier J., Kurobane Y., Packer J.A., Dutta D., Yeomans N., Design guide for circular hollow section (CHS) joints under predominantly static loading, CIDECT, 2008.

[2] Kato B., Hirose R., Bolted Tension Flanges Joining Circular Hollow Section Members, *Journal of Constructional Steel Research*, Vol5, No2, p79-101, 1985.

[3] Igarashi S., Wakiyama K., Inoue K., Matsumoto T., Murase Y., Limit design of high strength bolted tube flange joints: Part 1. Joint without rib-plates and ring-stiffeners, *Journal of structural and construction engineering*, Transactions of AIJ, Vol354, p52-66, 1985, (in Japanese).

[4] Couchaux M., Hjiaj M., Ryan I., Bureau A., Tensile resistances of bolted circular flange connections, *Engineering structures*, Vol 171, p817-841, 2018.

[5] Petersen, Ch., Stahlbau (Steel Construction), Braunschweig: Vieweg-Verlag, 1988.

[6] Seidel, M., Zur Bemessung geschraubter Ringflanschverbindungen von Windenergieanlangen, Institut für Stahlbau, Dissertation, Heft 20, Universität Hannover, 2001 (in German).

[7] Couchaux M., Ryan I., Hjiaj M., Bureau A., Tensile resistance of L-stubs, *Journal of Constructional Steel Research*, Vol 138, p131-149, 2017.

[8] Bourrier M., Lefeuvre M., anchorage of chimney, *Revue Construction Métallique*, N°3, CTICM, p66-70, 1976 (in French).

[9] Delesques R., Column bases of circular hollow section, *Revue Construction Métallique*, N°4, CTICM, p47-53, 1974 (in French).

[10] Yamaguchi T.E., Sugiura K., Mechanical behaviour of height strength bolted tube flange joints subjected to bending and tension, Proceedings of the 5th International colloquium on stability and ductility of steel structures, Nagoya, Japan, Vol1, p29-31, 1997.

[11] Stamatopoulos G., Ermopoulos J., Interaction curve for non-preloaded bolted connections in tubular members, Eurosteel 2008, 5th conference on steel and composite structures, Graz, Austria, p657-662, 2008.

[12] Stamatopoulos G., Non-preloaded Bolted ring flanges connections subjected to static loads, *International Journal of Steel Structures*, Vol 14, No2, p255-264, 2014.

[13] Kozlowski A., Wojnar A., Initial stiffness of flange bolted joints and their influence on the behaviour of steel chimneys, Eurosteel 2008, 5th conference on steel and composite structures, Graz, Austria, p663-668, 2008.

[14] Kozlowski A., Wojnar A., Mechanical model for assessment of the stiffness of bolted flange joint, Proceedings of the XIth International Conference on metal Structures, Rzeszow, Poland, 2006.

[15] Wojnar A., Kozlowski A., Sleczka L., Influence of the flange bolted joints stiffness on the behaviour of steel chimneys, The Third International Conference on Structural Engineering, Mechanics and Computation, Cape Town, South Africa, 2007.

[16] NF EN 14399-3: "High-strength structural bolting assemblies for preloading", CEN, 2015.

[17] NF EN 1090: Execution of steel structures and aluminium structures, Part 2: Technical requirements for steel structures, CEN, February 2009.

[18] Couchaux M., Behaviour of bolted circular flange connections, PhD Thesis, INSA of Rennes, November 2010 (in French).

[19] Yamaguchi T., Fundamental study on high strength bolted tensile joints, Dissertation of the Faculty of Engineering of Kyoto University, 1996.

[20] Jakubowski A., Schmidt H., Experimentelle Untersuchungen an vorgespannten Ringflanschstössen mit Imperfektionen, *Stahlbau*, Vol72, N°3, p188-197, 2003 (in German).

[21] Wang Y.Q., Zong I., Shi Y.J., Bending behaviour and design model of bolted flange-plate connections, *Journal of Constructional Steel Research*, Vol 84, p1-16, 2013.

[22] Pavlovic M., Heistermann C., Veljkovic M., Pak D., Feldmann M., Rebelo C., Da Silva L.S., Connections in towers for wind converters, part I: Evaluation of down-scaled experiments, *Journal of Constructional Steel Research*, Vol 115, p445-457, 2015.

[23] CECM-ECCS, recommended testing procedures for assessing the behaviour of structural elements under cyclic loads, European Convention for Constructional Steelwork, Technical Committee 1, TWG 13 – Seismic Design, No45, 1986.

[24] Couchaux M., Hjiaj., Ryan I., Bureau A., Effect of contact on the elastic behaviour of tensile bolted connections, *Journal of Constructional Steel Research*, Vol.133, p459-474, 2017.

[25] Couchaux M., Hjiaj M., Ryan I., Enriched beam model for slender prismatic solids in contact with a rigid foundation, *International Journal of Mechanical Sciences*, Vol. 93, p181-190, 2015.

[26] Eurocode 3, Design of steel structures – Part 1-8: Design of joints, CEN, 2005.

[27] Rotter J.-M., Sadowski A.-J., Development of circular tube slenderness classifications under axial and bending actions, Eurosteel 2017, Copenhaguen, September 2017.

[28] Eurocode 3, Design of steel structures, Part 1-6: Resistance and stability of shell, CEN, 2005.

[29] Draft of Eurocode 3, Design of steel structures – Part 1-1: General rules and rules for buildings, CEN, 2018.